Journal of Medicinal Chemistry

Article

pubs.acs.org/jmc

X-ray Absorption Near Edge Structure Spectroscopy to Resolve the in Vivo Chemistry of the Redox-Active Indazolium *trans*-[Tetrachlorobis(1*H*-indazole)ruthenate(III)] (KP1019)

Alfred A. Hummer,[†] Petra Heffeter,[‡] Walter Berger,[‡] Martin Filipits,[‡] David Batchelor,[§] Gabriel E. Büchel,[∥] Michael A. Jakupec,[∥] Bernhard K. Keppler,[∥] and Annette Rompel*[,†]

[†]Institut für Biophysikalische Chemie, Universität Wien, Althanstraße 14, 1090 Wien, Austria

[‡]Institut für Krebsforschung, "Comprehensive Cancer Center" und Forschungsplattform "Translational Cancer Therapy Research", Medizinische Universität Wien, Borschkegasse 8a, 1090 Wien, Austria

[§]Karlsruhe Institut für Technologie (KIT), ANKA, 76344 Eggenstein, Germany

[∥]Institut für Anorganische Chemie und Forschungsplattform "Translational Cancer Therapy Research", Universität Wien, Währinger Straße 42, 1090 Wien, Austria

Supporting Information

ABSTRACT: Indazolium *trans*-[tetrachlorobis(1*H*-indazole)-ruthenate(III)] (**1**, KP1019) and its analogue sodium *trans*-[tetrachlorobis(1*H*-indazole)ruthenate(III)] (**2**, KP1339) are promising redox-active anticancer drug candidates that were investigated with X-ray absorption near edge structure spectroscopy. The analysis was based on the concept of the coordination charge and ruthenium model compounds representing possible coordinations and oxidation states in vivo. **1** was investigated in citrate saline buffer (pH 3.5) and in carbonate buffer (pH 7.4) at 37 °C for different time intervals. Interaction studies on **1** with glutathione in saline buffer and apo-transferrin in carbonate buffer were undertaken, and the coordination of **1** and **2** in tumor tissues was studied too. The most likely coordinations and oxidation states of the compound under the above mentioned conditions were assigned. Microprobe X-ray fluorescence of tumor thin sections showed the strong penetration of ruthenium into the tumor tissue, with the highest concentrations near blood vessels and in the edge regions of the tissue samples.

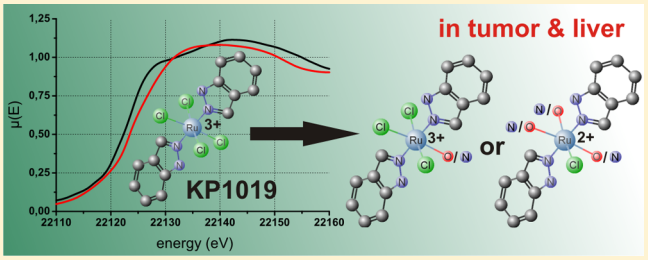

INTRODUCTION

Ruthenium compounds belong to the most promising candidates of non-platinum containing metal complexes for cancer therapy. Compared to Pt drugs Ru complexes cause less side effects and resistances against the drug are less likely.[1−3] The overall chemical and pharmacokinetic behavior of Ru is quite different from that of Pt compounds,[4] as reflected in extensive protein binding.[5,6] Imidazolium *trans*-[tetrachloro-(dimethylsulfoxide)(imidazole)ruthenate(III)] (**13**, NAMI-A),[7,8] indazolium *trans*-[tetrachlorobis(1*H*-indazole)ruthenate-(III)] (**1**, KP1019),[9−11] its sodium analogue sodium *trans*-[tetrachlorobis(1*H*-indazole)ruthenate(III)] (**2**, KP1339),[9−11] and Ru(II)-arene[12−17] complexes like [Ru(η^6-p-cymene)-Cl_2(pta)] (**14**, RAPTA-C, pta = 1,3,5-triaza-7-phosphatricyclo[3.3.1.1]decanephosphine)[18] are the most promising investigational drug candidates up to now. Phase I clinical trials in patients with refractory solid malignancies have successfully been completed for both **13**[19] and **1**,[20] the latter yielding disease stabilizations in more than half of the patients, and further clinical studies have commenced recently. In general, it is assumed that the Ru(III) complexes serve as prodrugs that are reduced under pathophysiological conditions to Ru(II).[21] **13** is a Ru(III) complex mainly active against metastases,[4,22] and it is assumed that its main site of action is located in the extracellular matrix.[23−25] The Ru(II)-arenes are organometallic complexes that are quite stable in the bloodstream, hydrolyzed in the nucleus, and bind to DNA.[16]

The Ru complexes **1** (Figure 1) and its Na salt analogue **2** (Figure 1) are the subject of investigation in this work. **1** and **2** differ only in their countercations, indazolium for **1** and Na^+ for **2**, exhibiting the same Ru(III) coordination sphere [tetrachlorobis(1*H*-indazole)ruthenate(III)]$^-$. Therefore, their main binding partners in vivo and their mode of action are thought to be very similar.[6,26] Both are showing antitumor activity exceeding that of Pt compounds or other cytostatic agents, e.g., in colorectal carcinomas in vivo and a variety of primary explanted human tumors in vitro.[1,20,26] Fast uptake of **2** by the cell and initiation of apoptosis (indicated by caspase activation) were observed.[6] The uptake mechanism of the two

Received: November 7, 2012
Published: January 3, 2013

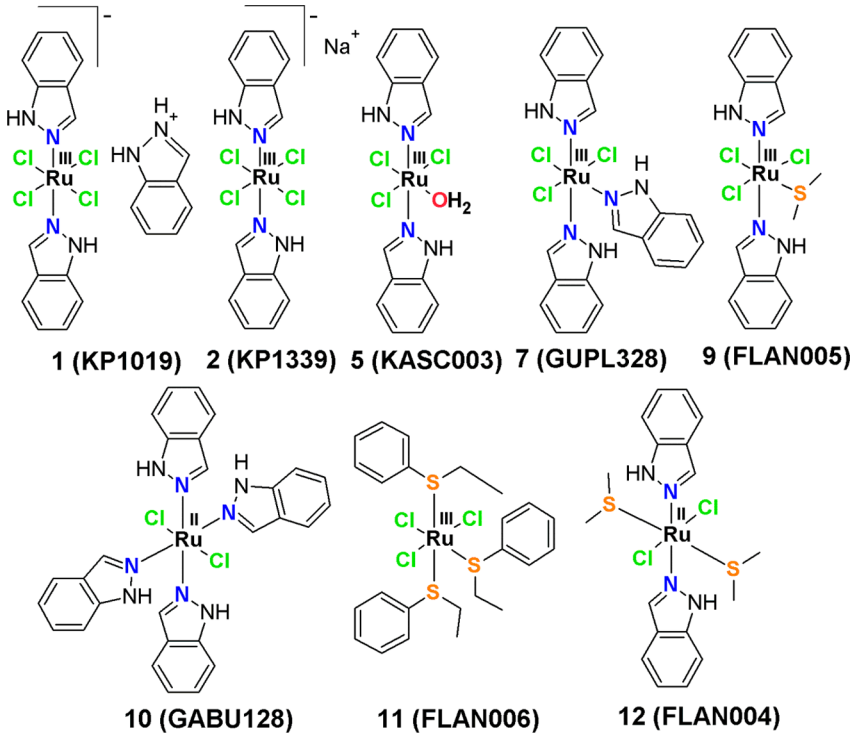

Figure 1. Structural formulas of the model compounds.

drugs may involve human serum albumin (HSA), the iron transport protein transferrin (Tf), and the Tf receptor, which is overexpressed in tumor cells to meet their increased demand for Fe.[27,28] A prodrug function is supposed involving reduction of Ru(III) to Ru(II),[21] which is supported by solution studies in the presence of different reductants.[29−31] Hypoxia is often seen in solid tumors because of insufficient tumor vascularization. The low oxygen level favors the reduction of Ru(III) and other redox-active substances.[21,27] The electrochemical potential of Ru(III)/Ru(II) is physiologically accessible, and glutathione (GSH) and single-electron transfer proteins are able to reduce Ru(III) in the presence of NADH.[27] However, the direct determination of the oxidation state, the coordination of the Ru active site, and the mechanism of action in vivo for these and other Ru drugs remains elusive.[24]

X-ray absorption spectroscopy (XAS)[32] is an element specific method that allows the investigation of the questioned element in disordered environments missing any long-range order. XAS has proven to be a valuable tool for the speciation of metal centers.[23,33−35] By application of X-ray absorption near edge structure (XANES) analysis, it is possible to determine the oxidation state and coordination of the Ru metal center, whereas extended X-ray absorption fine structure (EXAFS) analysis opens the opportunity to specify the identity, number, and distances of the adjacent atoms.[35] XAS is one method of choice to determine the oxidation state of the metal site in model compounds and especially of metal coordination sites in vivo. For instance Hambley et al.[36−38] could monitor activation by reduction of anticancer Pt(IV) compounds inside cells. New reduction pathways of Pt(IV) to Pt(II) species were monitored with XANES by Nemirovski et al.,[33] and the distribution and relative inertness of a Ga(III) compound in biological tissue were investigated in a previous publication.[39]

The main obstacle for bio-XAS is the low concentration of the metal in the targeted tissue. To generate spectra with a sufficiently good signal-to-noise ratio, X-ray sources like synchrotrons, with a sufficiently high photon flux in the range of 1×10^{11} to 4×10^{12} photons per second, are necessary. This high brilliance may cause the reduction of the probed metal through secondary electrons and the degradation of the biological tissue.[40−42] These effects can be minimized using low temperature sample environments like helium cooled cryostats at around 20 K.

Ascone et al.[43] studied the reaction of bovine serum albumin (BSA) with **13** and the formation of the respective **13**/BSA adducts by means of the sulfur and chlorine K-edges and the Ru K- and L_3-edges. Ru K- and L_3-edge spectra proved unambiguously that the Ru center remains in oxidation state +3 after protein binding. Comparative analysis of the Cl K-edge XAS spectra of **13** and **13**/BSA revealed that the Cl environment is greatly perturbed upon protein binding. In a subsequent study of Liu et al.[44] the binding behavior of **13** to BSA was analyzed by fitting a series of model compounds with known coordination to the unknown Ru(III)-BSA spectrum. The coordination environment of the adduct turned out to be completely different from that of the parent complex **13** with about 60% N and 40% O ligands coordinated to the Ru(III) center.

With a combination of S K-edge and Ru K-edge XAS and density functional theory (DFT) techniques Sriskandakumar et al.[45] studied the activation of Ru(II)-arene complexes through oxygenation and subsequent protonation of the thiolate (SR^-) ligand. The SR^- ligand is oxygenated to sulfinate (SO_2R^-) via sulfenate (SOR^-) and activated through protonation under acidic conditions. The protonation turned out to be a crucial step, which facilitates the dissociation of the SO_2R^- ligand and the DNA binding. The Ru metal center stayed in its Ru(II) state throughout this process and was not affected by the ligand oxygenation. Sadler and co-workers studied the photo-dissocation of Ru bipyridine complexes and their nucleobase

dx.doi.org/10.1021/jm301648f | J. Med. Chem. 2013, 56, 1182−1196

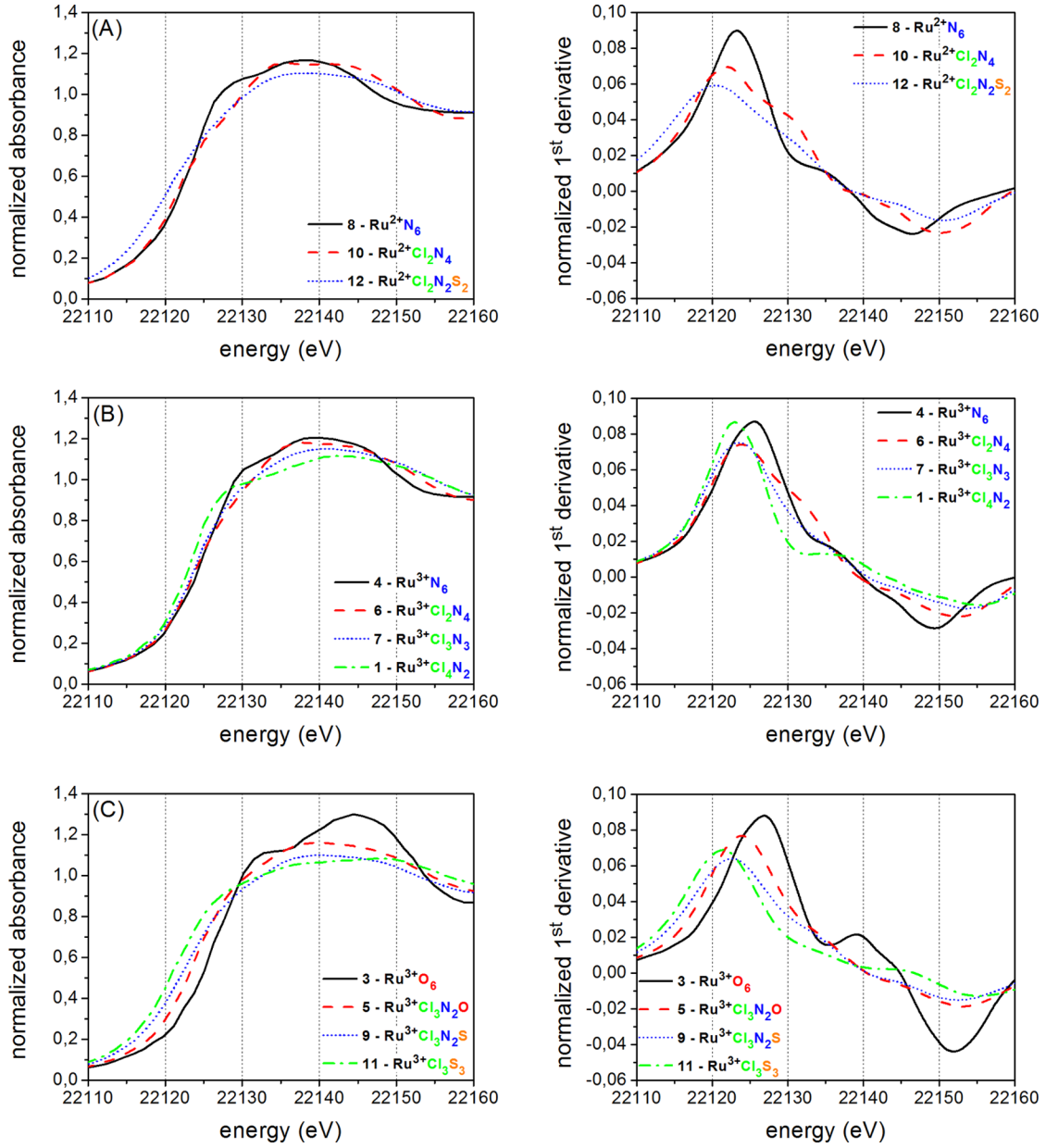

Figure 2. Normalized spectra of the model compounds and their corresponding first derivatives with a Ru(II) center (A), mixed Cl/N first shells (B), and O or S containing first shells (C).

binding with a combination of EXAFS and DFT calculations.[46−49] Harris et al.[50] used combined Cl K-edge and Ru L_3-edge XAS measurements together with DFT calculations to describe the electronic structure properties of a set of four Ru(III) and six Ru(II) complexes with mixed Cl/S/N coordination spheres, among them **1** and **13**. The effect of differing amounts of S (from dimethyl sulfoxide, DMSO) and N (from indazole/imidazole) ligands onto the electronic configuration within each Ru series (III and II) was quite low, and the ligand-to-metal donations reach a limit at around two S, two Cl, and two N ligands. This was ascribed to a so-called trans effect where the σ-donor and π-accepting effects of DMSO S ligands counteract each other. For **1** it was found that the indazole ligands are weaker donors toward Ru than imidazole ones, which is congruent with the proposed activation by reduction mechanism stated for **1** and its easier reduction to Ru(II) compared to the imidazole analogue *trans*-[tetrachlorobis(1*H*-imidazole)ruthenate(III)] (KP418).[30,51] Getty et al.[52] assigned Ru K-edge pre-edge peaks to the centrosymmetric structure of Ru carbene complexes for olefin metathesis. With increasing symmetry of the complexes the pre-edge peaks got weakened, which was ascribed to a lowered Ru 4d−5p orbital mixing.

Even though **1** and **2** are known to undergo hydrolysis (facilitating further ligand exchange reactions) and to be redox-active, both of which are features proposed to be significant for the mechanism of action, neither coordination nor redox condition of **1**/**2** after biotransformation in biological systems has been examined because of the lack of appropriate analytical methods. XAS is the method of choice that possesses a high value as a method for elucidation of the structure of metal coordination centers in biological environments. The aim of this work is to apply XAS to investigate the tumor-inhibiting Ru compound **1** in citrate saline buffer (CS buffer) at pH 3.5

dx.doi.org/10.1021/jm301648f | *J. Med. Chem.* 2013, 56, 1182−1196

within different time intervals, in the presence of the reducing agent GSH, in carbonate buffer in the presence of the possible transport protein apo-transferrin (apoTf), and as a powder. XANES spectra were recorded on tissue samples from mice treated with **1** and **2**. Micro X-ray fluorescence (micro-XRF) maps were taken from tumor tissue samples taken from mice treated with **2**. Additionally model compounds representing possible coordinations and oxidation states in vivo were measured as references. This study is designed to make a contribution toward the fundamental understanding of the biotransformation of Ru compounds in vivo and the underlying principle of "activation by reduction" which has to be evaluated.

RESULTS

XANES Spectra of the Model Compounds. The following model compounds were investigated with XAS: **1** (with first coordination shell $Ru(III)Cl_4N_2$),[9−11] ruthenium(III) acetylacetonate (**3**, $Ru(III)O_6$, Sigma Aldrich, CAS 14284-93-6, 97%),[53,54] hexammineruthenium(III) trichloride (**4**, $Ru(III)N_6$, Sigma Aldrich, CAS 14282-91-8, 99%),[55] *mer,trans*-aquatrichloridobis(indazole)ruthenium(III) (**5**, KASC003, $Ru(III)Cl_3N_2O$),[56] *trans,trans*-dichloridotetrakis(indazole)ruthenium(III) chloride (**6**, GABU129, $Ru(III)Cl_2N_4$),[27] *mer*-trichloridotris(indazole)ruthenium(III) (**7**, GUPL328, $Ru(III)Cl_3N_3$),[57] hexammineruthenium(II) dichloride (**8**, $Ru(II)N_6$, Sigma Aldrich, CAS 15305-72-3, 99.9%),[58] *mer,trans*-trichlorido(dimethylsulfide)bis(indazole)ruthenium(III) (**9**, FLAN005, $Ru(III)Cl_3N_2S$),[59] *trans,trans*-dichloridotetrakis(indazole)ruthenium(II) (**10**, GABU128, $Ru(II)Cl_2N_4$),[27] *mer*-trichloridotris(ethylphenylsulfide)ruthenium(III) (**11**, FLAN006, $Ru(III)Cl_3S_3$),[60] *trans,trans,trans*-dichloridobis(dimethylsulfide)bis(indazole)ruthenium(II) (**12**, FLAN004, $Ru(II)Cl_2N_2S_2$).[59] All spectra were collected at 20 K. The structural formulas are shown in Figure 1.

The XANES spectra of the model compounds and their corresponding first derivatives are presented in Figure 2. In Figure 2A the Ru(II) model compounds are shown. Figure 2B exhibits Ru(III) compounds with mixed Cl/N first shell ligand atoms (including **1**). Figure 2C displays compounds with O or S containing first shells. Within the same Ru oxidation state the edge energies increase with increasing electronegativity of the first shell atoms (see Table 1). Model compounds with the same first shells show an edge shift of about +2 eV from Ru(II) to Ru(III) (see **8**/**4** and **10**/**6**). The absence of any distinct pre-edge feature implies a centrosymmetric coordination of the here investigated Ru compounds.[52]

The edge energies observed in this study span a range of about 6 eV, with **1** occupying an energy position right in the middle. The bottom limit is marked by the S containing **12** in its oxidation state +2, and the upper boundary is represented by **3** with six O ligands and an oxidation state of +3. Comprising the highest amount of four Cl atoms, **1** occupies the lowest energy position within the Ru(III) models, exhibiting only Cl/N atoms in the first shells. The models **1**, **3**, and the Ru hexammine compounds **8** and **4**, in both oxidation states, exhibit a characteristic edge shoulder.

EXAFS Spectra of the Model Compounds. The k^3 weighted EXAFS spectra and the Fourier transforms (FT) of the Ru model compounds are shown in Figure 3. In Figure 3A the fine structures and the non-phase-shifted FT of the models containing a Ru(II) center are shown. Figure 3B shows the fine structures and FT of the Ru(III) compounds with mixed Cl/N first shells, and Figure 3C shows the one for the models containing O or S in their first shell around the Ru(III) center.

Table 1. Edge Energies and Calculated Coordination Charges of the Model Compounds, 1 in Solution, and the Liver and Tumor Samples[a]

compd	first coord shell	coord	edge energy [eV]	ΔE to **1** [eV]	η_{AR}
3	$Ru^{3+}O_6$	octah	22126.6	+3.3	+1.008
4	$Ru^{3+}N_6$	octah	22125.2	+1.9	+0.090
5	$Ru^{3+}Cl_3ON_2$	octah	22124.0	+0.7	−0.141
6	$Ru^{3+}Cl_2N_4$	octah	22124.0	+0.7	−0.166
7	$Ru^{3+}Cl_3N_3$	octah	22123.7	+0.4	−0.294
1	$Ru^{3+}Cl_4N_2$	octah	22123.3	±0.0	−0.422
8	$Ru^{2+}N_6$	octah	22123.0	−0.3	−0.910
9	$Ru^{3+}Cl_3N_2S$	octah	22122.7	−0.6	−0.588
10	$Ru^{2+}Cl_2N_4$	octah	22122.2	−1.1	−1.166
11	$Ru^{3+}Cl_3S_3$	octah	22121.3	−2.0	−1.176
12	$Ru^{2+}Cl_2N_2S_2$	octah	22120.5	−2.8	−1.754
1 in CS buffer		30 min	22124.4	+1.1	
1 in CS buffer		4 h	22124.4	+1.1	
1 in CS buffer		8 h	22121.9	−1.4	
1 with GSH/CS buffer		5 h	22122.0	−1.3	
1 in carb buffer		30 min	22125.2	+1.9	
1 with apoTf/carb buffer		30 min	22126.7	+3.4	
C1-liver (15 mg/kg of **1**)			22124.5	+1.2	
C1-tumor (15 mg/kg of **1**)			22124.4	+1.1	
B2-liver (7.5 mg/kg of **1**)			22124.4	+1.1	
B2-tumor (7.5 mg/kg of **1**)			22124.4	+1.1	
148-1-liver (40 mg/kg of **2**)			22124.4	+1.1	
148-1-tumor (40 mg/kg of **2**)			22124.5	+1.2	
B1-liver (40 mg/kg of **2**)			22124.4	+1.1	
F1-liver (40 mg/kg of **2**)			22124.4	+1.1	

[a] η_{AR} coordination charges calculated according to the Allred−Rochow scale.

The amplitudes of the fine structure oscillations and the FT magnitudes increase with a growing amount of heavy Cl and S scatterers. **11** shows the strongest *k*-space oscillations and FT magnitudes. For compounds with mixed N/O/Cl/S first shells and increasing number of N and/or O ligands a splitting of the first peak in the FT is observable. The Ru(II) compounds **10** and **12** have the largest Cl/N bond length differences and show the strongest peak splitting. The backscattering amplitudes of the heavy scatterers like S and Cl and the light scatterers like N and O are out of phase.[61] For **10** this cancellation leads to a node between 7 and 9 $Å^{-1}$ seen in Figure 3A (red dashed curve). The Ru(III) analogue **6** has the same features between 8 and 10 $Å^{-1}$ seen in Figure 3B (red dashed curve). The shift of this feature is mainly attributed to the shortened Cl bond lengths of the higher oxidized **6**.

The fitting analysis using FEFF[62,63] was restricted to the first coordination shell extracted from the first peak in the FT. The

dx.doi.org/10.1021/jm301648f | J. Med. Chem. 2013, 56, 1182−1196

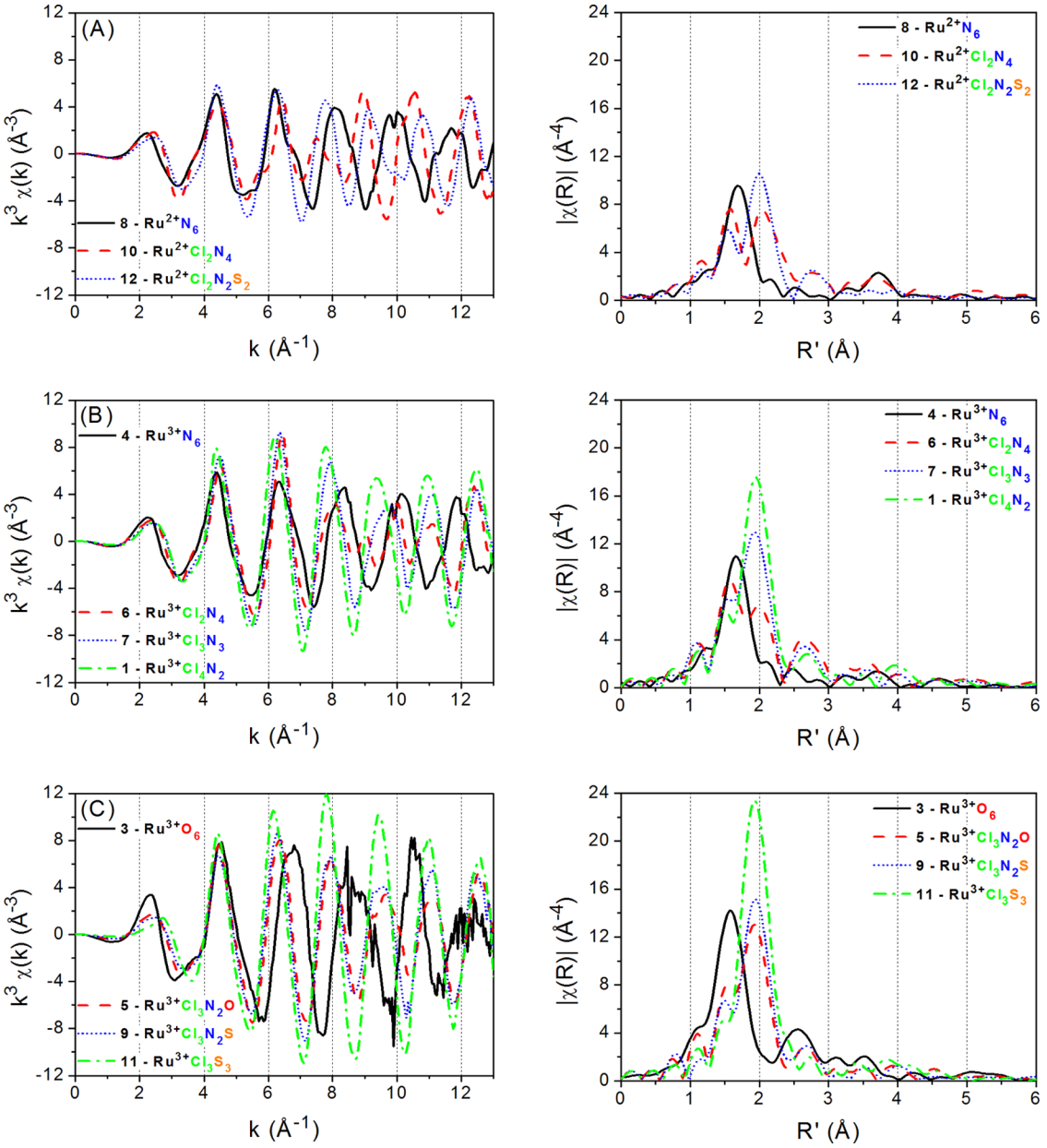

Figure 3. Extracted fine structures and Fourier transforms of the model compounds with a Ru(II) center (A), a mixed Cl/N first shell (B), and a O or S containing first coordination shell (C).

identity and number of backscatterers were fixed to the crystallographic values not to exceed the number of fitting parameters, and the known distances were taken as a starting point for the fitting analysis. The results of the first shell fits of the model compounds using theoretical amplitudes and phases provided by the FEFF code are presented in the Supporting Information (Table S2), as well as the results for the DL-EXCURV[64] fits (Table S3). The distances are given as the average fitted distances for each atom type/shell (Cl/S, O/N, and N/C). For **6** and **10** the second shell scatterers 4 N and 4 C at about 3 Å were included in the FEFF fit, as they had a significant influence on the first shell spectral features. The curve fitting results obtained by FEFF and DL-EXCURV are both in good agreement with the crystallographic data. Thus, the reliability of the amplitude and phase shift extracted from the model compounds is confirmed.

Coordination Charge versus Edge Position. In previous articles a correlation between the coordination charge and a distinct spectral edge feature could be shown.[65−69] In this study the edge position determined over the first maximum in the first derivative was chosen as the point of reference. The electronegativity values according to the Allred/Rochow tables were used in the calculations.[70] The calculated ionicities and corresponding degrees of covalence of the elements occurring in the first shells of the models are presented in Table 2. In Table 1 the coordination charges and corresponding edge energies are listed. The ruthenium model compounds are listed in order of their observed edge positions. In Figure 4 the calculated coordination charges versus the experimentally determined Ru K-edge positions are shown.

The edge energy of **1** in boron nitride (BN) was set as an arbitrary origin and lies right in the middle of the observed edge energy range. A straight line was regressed with a coefficient of

dx.doi.org/10.1021/jm301648f | J. Med. Chem. 2013, 56, 1182−1196

Table 2. Calculated Ionicities I_{AR} and Covalencies c_{AR} for O, N, Cl, and S According to the Allred–Rochow[70] Scale[a]

			Allred–Rochow	
element	Z	χ_{AR}	I_{AR}	c_{AR}
oxygen	8	3.5	0.668	0.332
nitrogen	7	3.1	0.515	0.485
chlorine	17	2.8	0.387	0.613
sulfur	16	2.4	0.221	0.779

[a] Z, atomic number; χ_{AR}, electronegativity according to Allred–Rochow; I_{AR}, calculated ionicity; c_{AR} calculated covalency.

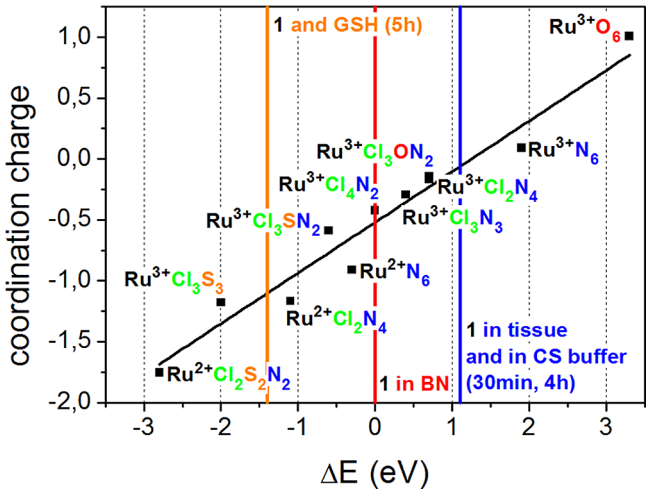

Figure 4. Calculated coordination charge η_{AR} according to the Allred–Rochow scale in comparison to the observed edge energies of the XANES spectra.

determination R^2 = 0.95, demonstrating a linear correlation between the coordination charge and the edge positions. The compounds containing Ru(II) and/or S are on the left (lower energy) side, and the compounds containing Ru(III), N, and O are on the right (higher energy) side. This correlation is the basis for the further interpretation of the coordination mode of Ru compounds in biological samples and in the presence of potential transport proteins.

XANES Spectra of 1 in CS Buffer (pH 3.5, 30 min, 4 h, 8 h, 5 h with GSH). In Figure 5A the XANES spectra of **1** in BN, suspended in CS buffer and in the presence of GSH (5-fold excess, CS buffer, pH 3.5), are shown. **1** was incubated at 37 °C for 30 min, 4 h, 8 h, and 5 h in the presence of GSH. The spectra of **1** after 30 min and 4 h of incubation are shifted by +1.1 eV to higher energies than **1** in BN. After 8 h of incubation of **1** in CS buffer and 5 h in the presence of GSH, both spectra are shifted significantly to lower energies by −1.4 and −1.3 eV, respectively. The CS buffer spectra, after 30 min and 4 h, lost the edge shoulder at 22 130 eV present in the solid sample of **1**. The nearest model compound edge positions to these solution spectra (ΔE = +1.1 eV) are those with Ru(III)Cl_2N_4 and Ru(III)Cl_3ON_2 first coordination shells. The shift in energy suggests that an average exchange of one Cl ligand with an O atom arising from the buffer solution or a N atom from indazole (deprotonated indazolium) took place. The indazolium cation has a pK_a of 1.25 which enables deprotonation and opens the possibility to act as a N donor at pH 3.5. This coordination environment proved to be stable up to 4 h, and the reduction to Ru(II) is not assumed. In the Ru(II) state an edge shift of +1.1 eV would only be possible through the exchange of all ligands by O arising from the buffer solution. The spectrum of **1**, after 8 h, is shifted to lower energies by −1.4 eV. In comparison to the solution spectrum of **1** after 4 h a shift of −2.5 eV is seen. This demonstrates fundamental changes in the first coordination environments around the Ru center. In the presence of GSH the spectrum is shifted to the low energy positions in the region of the Ru(II) and Ru(III) S containing model compounds. Least square fits (LSF) were performed to suggest the most likely first coordination modes.

LSF of 1 in CS Buffer (pH 3.5, 30 min, 4 h, 5 h with GSH). LSF to **1** in CS buffer (30 min, 4 h) and in the presence of GSH (5 h) was performed using the solid state spectra of **1**, **4**, **5**, **6**, **9**, **10**, and **12**. The fit results are shown in Table 3 and were analyzed according to the goodness of fit parameters χ^2 and χ^2_{red}, the shift in energy ΔE, and the scaling factor Σ_C. The best fits for each sample are highlighted in bold-face. The best fits to **1** (30 min, 4 h) could be achieved with **5**. An exchange of an average of one Cl atom for an O from the buffer solution or N from indazole (deprotonated countercation) are two possible scenarios. In the presence of GSH the spectra of **9** and **12** gave similar results in the goodness of fit parameters but with opposite edge shift variances. This points toward a Ru(II)$(Cl/S)_4N_2$ coordinated species, which would best match the experimental data, but a Ru(III)ClS_3N_2 cannot be ruled out.

XANES Spectra of 1 in Carbonate Buffer (pH 7.4, 30 min without and with apoTf). In Figure 5B the normalized XANES spectra and first derivatives of **1** suspended in carbonate buffer (30 min, 37 °C) and in carbonate buffer in the presence of apoTf (30 min, 37 °C) are shown. For comparison the spectrum of **1** in CS buffer (pH 3.5) is shown as well. The spectrum of **1** in carbonate buffer is shifted by +1.7 eV to higher energies, which is slightly more than **1** in CS buffer (+1.1 eV). The spectrum of **1** in the presence of apoTf is shifted even further to a higher energy position (+3.3 eV). This immense shift to positive energies is mostly due to the change in edge shape. When introducing a horizontal line at the ordinate value corresponding to the edge energy of the carbonate buffer spectra, a change to the apoTf spectrum results in an energy displacement of about +0.5 eV. This suggests the exchange of additional Cl ligands by O or N, thus resulting in a first shell with a high content in O/N in the presence of apoTf (see Figure 7).

LSF of 1 in Carbonate Buffer (pH 7.4, 30 min without and with apoTf). LSF on **1** in carbonate buffer (30 min) and in the presence of apoTf (30 min) was done in the same way as described for **1** dissolved in CS buffer. The best fitting results are highlighted in boldface in Table 3. The best fits to **1** in the carbonate buffer solution were achieved with **5** and **6**. In the presence of apoTf the best fit was attained with a coordination of Ru(III)Cl_2N_4. Proposed structural motifs are presented in Figure 7. In a subsequent step linear combination analysis (LCA) was performed on the solution spectra.

LCA of Solution Spectra with 3, 4, and 11. LSF of **3**, **4**, and **11** and combinations of them has been performed on **1** in BN, **1** in CS buffer at pH 3.5 (4 and 5 h with GSH), and **1** in carbonate buffer at pH 7.5 (30 min with and without apoTf). **11** was taken as a model for a $RuCl_6/S_6$ species. The LCA with RuO_6, RuN_6, and $RuCl_3S_3$ environments resembles the known first coordination shell of solid **1** very well. After 4 h in CS buffer at 37 °C a decrease to an overall coordination of Ru to about 3 N and 3 Cl in solution is seen by LCA. After an incubation of 5 h in CS buffer in the presence of GSH a ratio of 2 N to 4 Cl/S gave the best fitting results. In the presence of

dx.doi.org/10.1021/jm301648f | J. Med. Chem. 2013, 56, 1182–1196

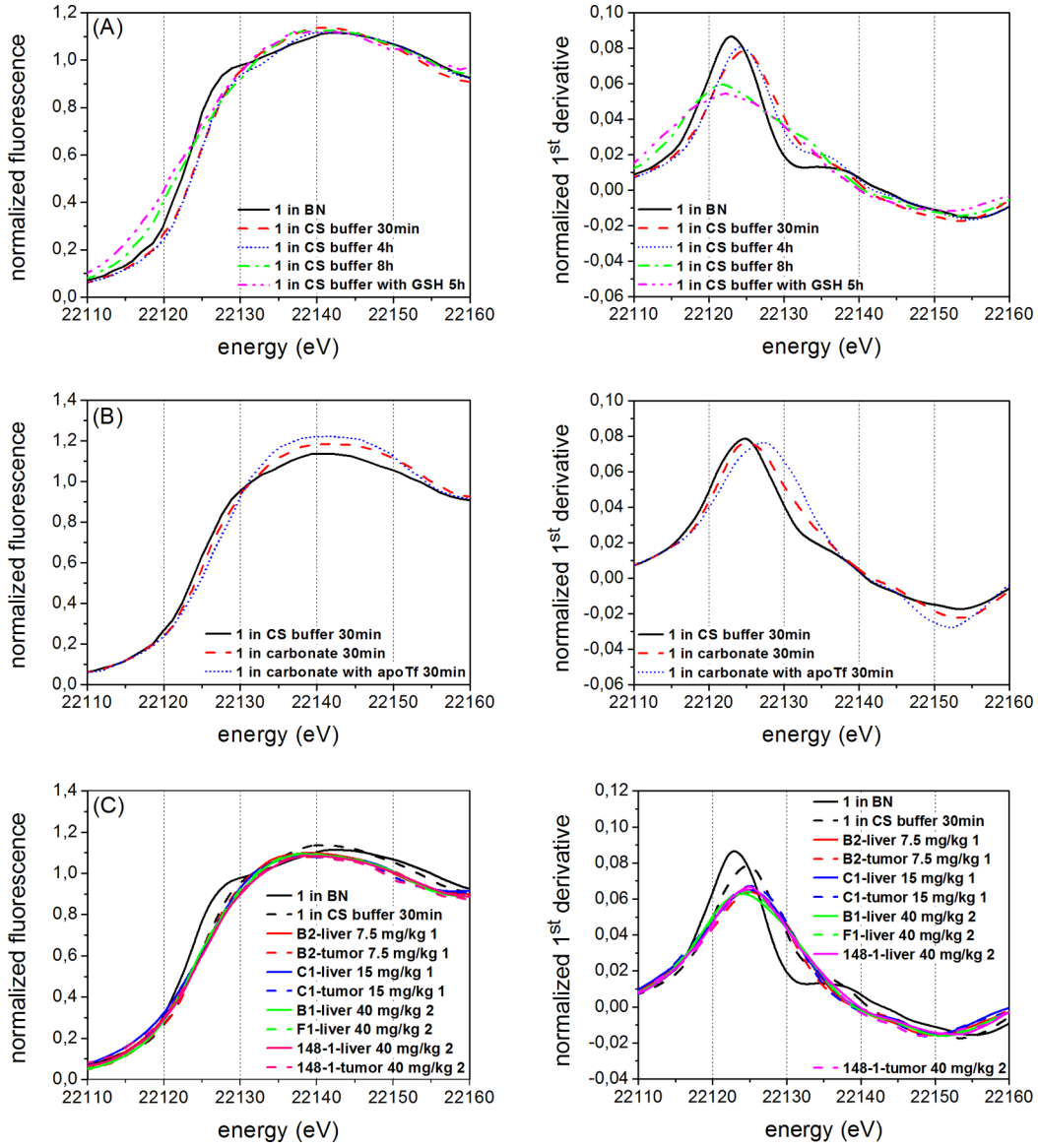

Figure 5. (A) Normalized XANES spectra and first derivative of **1** in BN, **1** in CS buffer (after 30 min, 4 h, and 8 h) and in CS buffer in the presence of the reducing agent GSH (after 5 h). (B) **1** in CS buffer (30 min) and carbonate buffer (30 min) and in carbonate buffer in the presence of apoTf (30 min). (C) Normalized XANES spectra and first derivatives of the tumor and liver samples.

apoTf the best LCA fits were obtained with a first shell environment dominated by O/N and a small proportion of Cl. The proposed first shell coordinations are presented in Figure 7, and the fitting results are shown in the Supporting Information (Table S4).

XANES Spectra of the Tissue Samples. XANES spectra of tumor and liver samples from mice treated with **1** or **2** were collected in fluorescence mode at 20 K with an unfocused beam. Because of the low concentration of Ru in the biological tissue, data collection was restricted to the XANES region. The normalized XANES spectra and the corresponding first derivatives of the tumor and liver samples from mice are shown in Figure 5C. The samples were taken from mice treated with different concentrations and application schemes of **1** and **2** (details for drug administration see Supporting Information).

The edge positions of the XANES spectra taken from all tumor and liver material are around 22 124.4 eV within 0.1 eV deviation (see Table 1). Because of the low signal strength, the changes in the edge positions are within the statistical error and there is no evidence for a change in comparison of all measured tissue spectra. The Ru K-edge XANES spectra taken from liver and tumor samples are highly similar, which indicates the same local coordination around the Ru center. The apparent coordination charge of the Ru center of **1** and **2** in the tissue is similar to **1** in CS buffer after 30 min and 4 h of incubation at 37 °C. Principal component analysis (PCA) was performed to confirm the high similarities seen within the probed tissue samples. LSF was used to propose a possible coordination and oxidation state pairing for the chemical constitution in tissue.

PCA and LSF of the Tissue Samples. In the following tissue XANES spectra were studied applying PCA to give a statistical foundation for possible coordinations in vivo.[71] PCA was performed taking all tissue sample spectra into account. The variance within all tissue samples could be described to an extent of 98% with the first principal component. The target transforms of the model compounds **1**, **4**, **5**, **6**, and **7** to the vector subspace of the first principal component are presented in the Supporting Information (Figure S1, not for **4**).

dx.doi.org/10.1021/jm301648f | J. Med. Chem. 2013, 56, 1182−1196

Table 3. LSF of Model Compounds 1, 4, 5, 6, 9, 10, and 12 to the Spectrum from 1 Suspended in CS Buffer (30 min, 4 h) in the Presence of GSH in CS Buffer (5 h) and in the Presence of apoTf (30 min)[a]

		model compounds						
		1	**4**	**5**	**6**	**9**	**10**	**12**
1 in CS buffer 30 min	χ^2	1.212	1.343	**0.173**	0.740	1.077	1.030	1.645
	χ^2_{red}	0.00061	0.00067	**0.00008**	0.00037	0.00054	0.0051	0.00082
	ΔE	−1.06	0.38	**−0.21**	−0.23	−1.28	−1.40	−2.98
	Σ_C	1.0076(6)	0.9862(7)	**0.9919(2)**	0.9957(5)	1.0258(6)	1.0037(6)	1.0147(7)
1 in CS buffer 4 h	χ^2	0.347	2.777	**0.347**	1.607	0.599	1.811	1.474
	χ^2_{red}	0.00017	0.00140	**0.00017**	0.00080	0.00030	0.00091	0.00074
	ΔE	−1.27	0.17	**−0.47**	−0.53	−1.57	−1.70	−3.21
	Σ_C	0.9920(3)	0.970(1)	**0.9764(3)**	0.9801(7)	1.0104(5)	0.9884(8)	1.0014(7)
1 with GSH in CS buffer 5 h	χ^2	3.406	6.447	2.774	3.798	**0.811**	3.262	**0.685**
	χ^2_{red}	0.00170	0.00323	0.00139	0.00190	**0.00041**	0.00163	**0.00034**
	ΔE	0.91	2.02	1.64	1.61	**0.66**	0.54	**−1.10**
	Σ_C	1.000(1)	0.980(1)	0.9851(9)	0.988(1)	**1.0190(5)**	0.996(1)	**1.0094(5)**
1 in carb buffer 30 min	χ^2	2.452	1.317	**0.331**	**0.312**	1.745	0.945	2.371
	χ^2_{red}	0.00123	0.00066	**0.00017**	**0.00016**	0.00087	0.00047	0.00119
	ΔE	−1.80	−0.49	**−0.99**	**−1.02**	−2.02	−2.13	−3.79
	Σ_C	1.0185(9)	0.9982(6)	**1.0032(3)**	**1.0072(3)**	1.0369(8)	1.0149(5)	1.0275(9)
1 with apoTf in carb buffer 30 min	χ^2	5.650	0.961	1.894	**0.648**	4.238	1.618	6.878
	χ^2_{red}	0.00283	0.00048	0.00095	**0.00032**	0.00212	0.00081	0.00344
	ΔE	−2.12	−0.87	−1.32	**−1.29**	−2.19	−2.18	−2.93
	Σ_C	1.028(1)	1.0093(6)	1.0134(8)	**1.0174(5)**	1.046(1)	1.0242(7)	1.031(1)

[a] χ^2 is the goodness of fit parameter scaled to the estimated uncertainty. χ^2_{red} is χ^2 divided by the number of free parameters. ΔE accounts for the energy shift of the sample data. Σ_C is the sum of the fitted components and is the scaling factor applied to the fitted spectrum. The best fit is highlighted in boldface.

Obviously **1** and **4** gave the worst results with SPOIL factors of 10.22 and 9.00, which are well above an acceptable value. As described in Webb et al.[72] and in Malinowski et al.,[73] a SPOIL factor below 6 is acceptable and below 3 would be a good result.

The model compounds **7**, **5**, and **6** reach values of 4.95, 5.31, and 5.49, respectively (see Table 4). All other reference compounds measured in this study are far away from an acceptable result. On basis of the target transformation results, LSF to each tissue sample was conducted. The outcomes of the LSF of **4**, **5**, **6**, and **7** to the tissue sample spectra are summarized in Table 5. Fits based on solid **1** to each tissue sample are included in this study as well. The best values based on the statistical misfit χ^2, χ^2_{red}, and energy shift ΔE were achieved with **5** and **7**. These two fits are nearly identical, whereas **5** shows the smallest edge shift and **7** a lower statistical misfit. The fits with **6** are slightly worse in all fitting parameters. During the fits, the samples were shifted in energy with respect to the reference compounds. The shift in energy ΔE of the fitted samples was between −0.39 and +0.39 eV. The fits of **5** to B2-liver and B2-tumor are coplotted in the Supporting Information (Figure S2).

Table 4. Target Transformations of 1, 4, 5, 6, and 7[a]

parameter	**1**	**4**	**5**	**6**	**7**
χ^2	1.463	1.162	**0.413**	0.438	**0.336**
R_{value}	0.00186	0.00144	**0.00051**	0.00055	**0.00045**
SPOIL	10.22	8.99	**5.31**	5.49	**4.95**

[a] χ^2 is the goodness of fit parameter scaled to the estimated uncertainty. R_{value} is a measure of the percent misfit. SPOIL factor is an arbitrary defined value for the goodness of fit and should be below 6. The best fit is highlighted in boldface.

The edge position of the tissue samples is indicated by the vertical blue line in Figure 4. This shift is slightly above the one for **5** and **6**. For the tissue samples Ru(III)Cl_3N_2(O/N) is proposed as a possible first shell environment for the majority of the **1** and **2** molecules, which are dominating the XAS signals. Nevertheless a Ru(II) species with a high O and/or N content in the first coordination sphere as in Ru(II)ClN_2(O/N)$_3$ cannot be ruled out.

Micro-XRF Maps of the Tissue Samples. Tumor (SW480) samples of mice treated with **2** were scanned with a X-ray beam focused to 10 μm. The resulting maps give an overview of the elemental distribution patterns of ruthenium, iron, copper, and zinc in a defined region of the tumor. In Figure 6 the 924 × 660 μm^2 micro-XRF maps of Ru, Fe, Cu, and Zn of one SW480 tumor (mouse 148-1) sample are presented. The scanned region is indicated by a rectangle in the pictures in the top row. Picture A is the scanned 10 μm thin section on Ultralene film, and picture B is the consecutively cut hematoxylin and eosin (H & E) stained 5 μm thin section mounted on a glass slide. The concentrations of all four elements are highest in the region of the blood vessels and in the edge regions of the tissue. The concentrations drop when going into the closer packed tissue regions. In contrast to the Fe, Cu, and Zn distribution, Ru shows a more disperse pattern with hotspots apart from the predominantly higher concentrated areas. The correlation between the Ru distribution pattern and the Fe one is of the same order of magnitude as between Ru/Cu or Ru/Zn. This opens the question of whether physiological pathways other than the Fe-dependent ones are involved in the Ru transport as well.

DISCUSSION

XANES analysis has been applied to propose a first coordination environment of an investigational anticancer

dx.doi.org/10.1021/jm301648f | J. Med. Chem. 2013, 56, 1182−1196

Table 5. LSF of Model Compounds 1, 4, 5, 6, and 7 to Tissue Sample Spectra from Mice Treated with 1 or 2[a]

	1	4	5	6	7
			B2-Liver, 7.5 mg/kg **1**		
χ^2	2.244	1.447	**0.696**	0.671	**0.605**
χ^2_{red}	0.00112	0.00072	**0.00035**	0.00034	**0.00030**
ΔE	−0.70	0.73	**0.20**	0.24	**−0.17**
Σ_C	0.9688(9)	0.9485(7)	**0.9536(4)**	0.9568(5)	**0.9583(4)**
			B2-Tumor, 7.5 mg/kg **1**		
χ^2	1.974	1.749	**0.953**	1.124	**0.817**
χ^2_{red}	0.00099	0.00087	**0.00048**	0.00056	**0.00041**
ΔE	−0.94	0.59	**−0.01**	0.04	**−0.39**
Σ_C	0.9680(8)	0.9469(8)	**0.9523(6)**	0.9555(6)	**0.9571(5)**
			C1-Liver, 15 mg/kg **1**		
χ^2	2.634	2.464	**1.214**	1.374	**1.030**
χ^2_{red}	0.00132	0.00123	**0.00061**	0.00069	**0.00052**
ΔE	−0.58	0.85	**0.34**	0.39	**−0.03**
Σ_C	0.9690(9)	0.9486(9)	**0.9537(6)**	0.9568(7)	**0.9583(6)**
			C1-Tumor, 15 mg/kg **1**		
χ^2	2.339	1.643	**0.988**	1.096	**0.877**
χ^2_{red}	0.00117	0.00082	**0.00049**	0.00055	**0.00044**
ΔE	−0.85	0.64	**0.11**	0.17	**−0.27**
Σ_C	0.9621(9)	0.9414(7)	**0.9464(6)**	0.9495(6)	**0.9512(5)**
			B1-Liver, 40 mg/kg **2**		
χ^2	2.097	1.580	**0.728**	0.679	**0.591**
χ^2_{red}	0.00105	0.00079	**0.00036**	0.00034	**0.00030**
ΔE	−0.76	0.62	**0.08**	0.08	**−0.30**
Σ_C	0.9657(8)	0.9455(7)	**0.9525(5)**	0.9543(5)	**0.9555(5)**
			F1-Liver, 40 mg/kg **2**		
χ^2	2.070	1.534	**0.660**	0.634	**0.523**
χ^2_{red}	0.00104	0.00077	**0.00033**	0.00032	**0.00027**
ΔE	−0.72	0.70	**0.14**	0.16	**−0.23**
Σ_C	0.9681(8)	0.9477(7)	**0.9530(5)**	0.9564(5)	**0.9577(4)**
			148-1-Liver, 40 mg/kg **2**		
χ^2	1.871	1.874	**0.713**	0.910	**0.523**
χ^2_{red}	0.00094	0.00094	**0.00036**	0.00046	**0.00026**
ΔE	−0.96	0.47	**−0.09**	−0.09	**−0.47**
Σ_C	0.9627(8)	0.9421(8)	**0.9475(5)**	0.9509(6)	**0.9523(4)**
			148-1-Tumor, 40 mg/kg **2**		
χ^2	2.680	1.820	**1.156**	1.016	**0.987**
χ^2_{red}	0.00134	0.00091	**0.00058**	0.00051	**0.00049**
ΔE	−0.70	0.71	**0.20**	0.22	**−0.17**
Σ_C	0.955(1)	0.9343(8)	**0.9393(6)**	0.9427(6)	**0.9441(6)**

[a] χ^2 is the goodness of fit parameter scaled to the estimated uncertainty, red. χ^2_{red} is χ^2 divided by the number of free parameters. ΔE accounts for the energy shift of the sample data, and Σ_C is the sum of the fitted components and is the scaling factor applied to the fitted spectrum. The best fit is highlighted in boldface.

drug in CS buffer (pH 3.5) and carbonate buffer (pH 7.4), in carbonate buffer in the presence of apoTf, in CS buffer in the presence of GSH, and in the target tissue. The concept of the coordination charge was applied to the model compounds, and a linear correlation between the coordination/oxidation state and the observed edge energies was established. This was the basis for the further interpretation of the spectra of **1** in solution and in biological samples. The proposed oxidation states and coordinations are summarized in Figure 7.

1 in CS Buffer (30 min, 4 h, and 8 h, pH 3.5) and Carbonate Buffer (30 min, pH 7.4). The spectra collected on **1** suspended in CS buffer (30 min, 4 h at 37 °C, pH 3.5) suggest the dissociation of an average of one Cl ligand and a change of the first shell environment from $Ru(III)Cl_4N_2$ to $Ru(III)Cl_3ON_2$. This coordination turned out to be prevalent up to 4 h of incubation, and **1** is suggested to remain in its oxidation state Ru(III). This can be interpreted by an average exchange of one Cl ligand for an O atom from the buffer solution or a N atom from indazole formed by deprotonation of the indazolium cation at pH 3.5. A possible N coordination is unique for **1** because of its chemical composition including an indazolium countercation. After 8 h in CS buffer at 37 °C a significant change in the XANES spectra was seen, which is proof of a further transformation of the compound in solution. At pH 7.4 and 37 °C in carbonate buffer, the results of this XAS study are pointing toward an average exchange of at least one Cl ligand after 30 min of incubation as well. The Cl ligand can be exchanged for an O atom arising from water, an O atom from carbonate, or a N ligand from indazole. Compared to the 1 mM concentrated indazolium countercation, the possible O donors are much higher concentrated in the buffer solution. The hydrolyzing reactions of **1** were studied previously by high

dx.doi.org/10.1021/jm301648f | J. Med. Chem. 2013, 56, 1182−1196

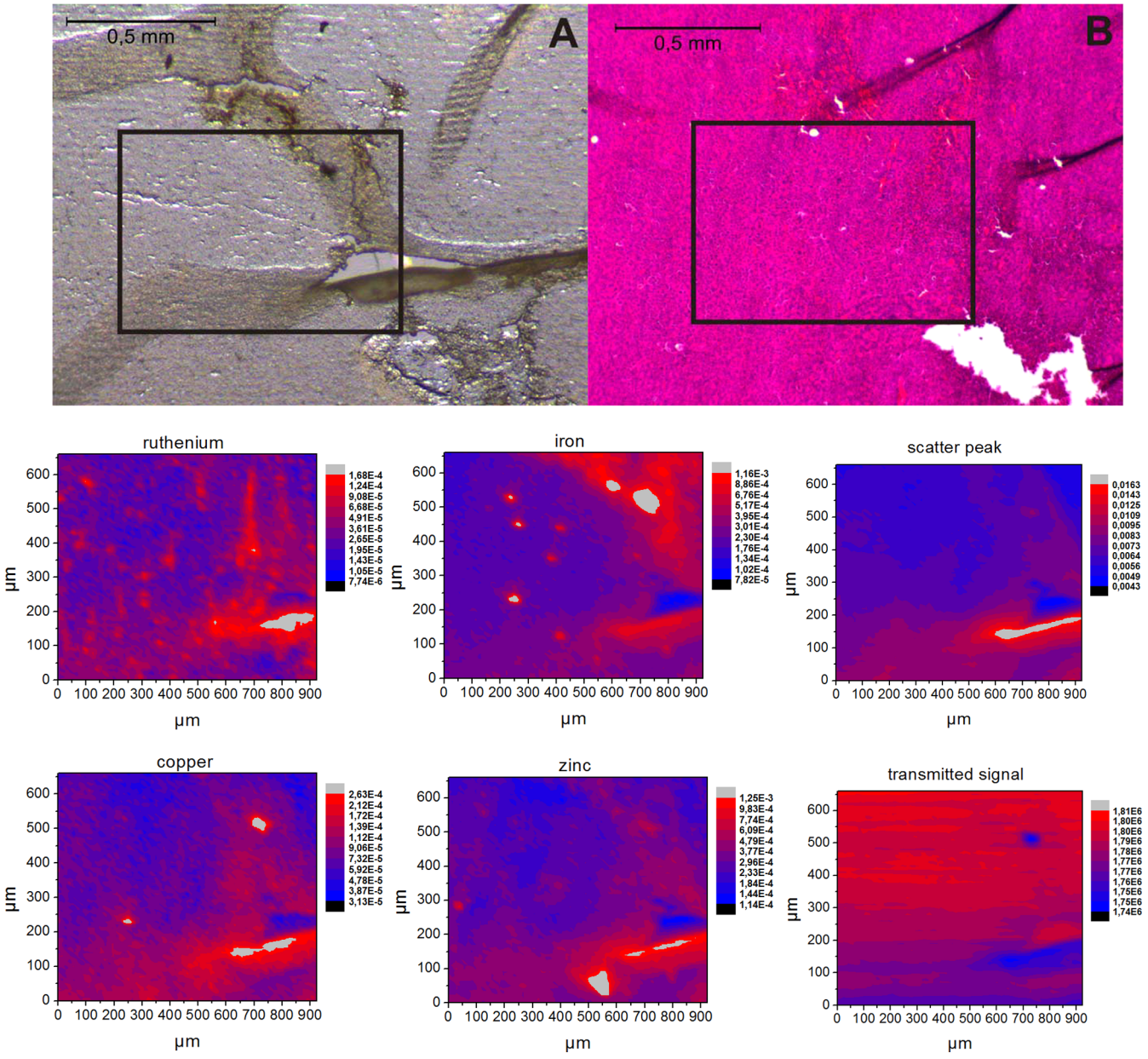

Figure 6. Micro-XRF maps of Ru, Fe, Cu, and Zn. The scanned regions are indicated by the rectangle in the pictures in the top row. The scatter peak and the transmitted signal (the data show a total variation of ≤3%) are shown as well. In the top left is shown a picture of the scanned 10 μm thin section. In the top right is shown a picture of the consecutively cut H & E stained 5 μm thin section.

performance capillary electrophoresis (HPCE), high performance liquid chromatography−mass spectrometry (HPLC−MS), and capillary zone electrophoresis inductively coupled plasma mass spectrometry (CZE-ICP-MS).[74,75] **1** turned out to be the most labile complex in comparison to **13** and **14**.[75] The half-life of **1** in buffer solution (10 mM phosphate buffer, 100 mM NaCl, pH 7.4) was determined to be 17.1 min.[75] In water **1** was hydrolyzed to about 2% within 2 h. The half-life in buffered solutions at 37 °C turned out to be much smaller with values of 5.5 h (pH 6.0) and <0.5 h (pH 7.4).[74] Altogether the stability of **1** is strongly dependent on the pH of the buffer used, with the highest stability in solutions of low pH.[74]

1 in the Presence of GSH (CS Buffer, pH 3.5). Ru(III), like Pt(IV), can be reduced by GSH under physiological conditions, and the resulting Ru(II) complexes maintain their octahedral ligand set.[24,76] An energy shift of −1.4 eV in comparison to solid **1** was found after 5 h of incubation in CS buffer in the presence of GSH (5-fold excess, 37 °C, pH 3.5). Because of the 5-fold excess of GSH and the shift to lower energies, an adduct formation between **1** and GSH accompanied by a reduction to Ru(II) is very likely, with a first coordination environment of $Ru(II)Cl_3SN_2$. An unchanged Ru(III) center with a $Ru(III)ClS_3N_2$ coordination would also match the seen shift in energy (see Figure 7). Reduction by GSH has previously been reported for $[Cr(VI)O_4]^{2-}$ to a GSH bis-ligated chromium(V)-GSH complex.[23]

1 in the Presence of apoTf (Carbonate Buffer, pH 7.4). **1** binds to Tf and is released from the protein supposedly after reduction to Ru(II) by biological reductants, and the interference with the Fe metabolism is assumed.[24,76,77] In the presence of apoTf, **1** incubated for 30 min in carbonate buffer (pH 7.4) shows a slightly higher edge position than **1** in

dx.doi.org/10.1021/jm301648f | J. Med. Chem. 2013, 56, 1182−1196

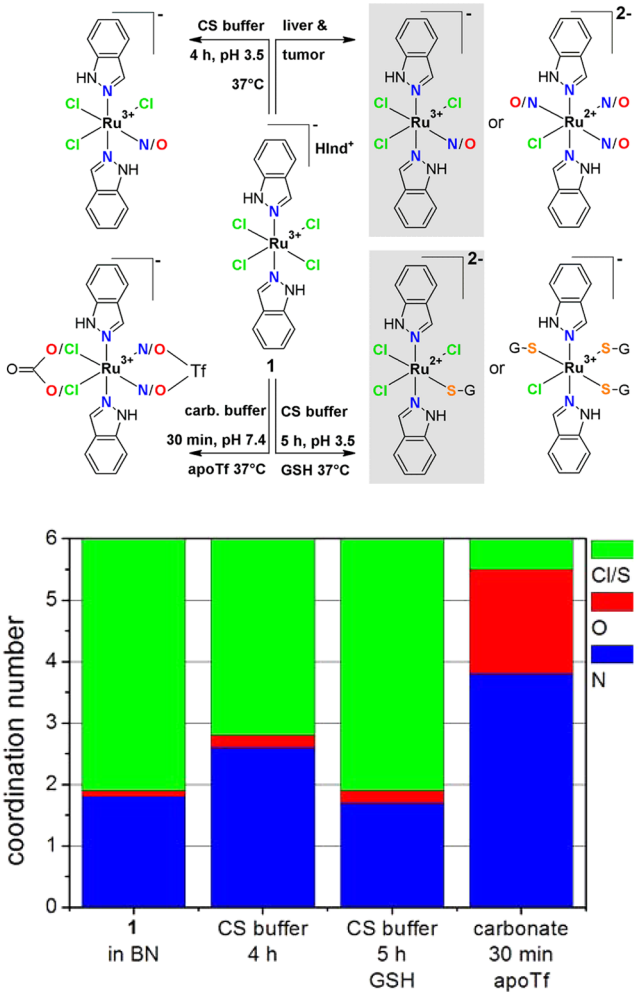

Figure 7. Proposed oxidation state and first shell coordination of **1** in CS buffer (4 h), in liver and tumor tissue, in CS buffer in the presence of GSH and in carbonate buffer in the presence of apoTf (top). Results are from LCA analysis (bottom).

carbonate buffer without apoTf. This is explainable by the exchange of additional Cl through O and/or N ligands, whereas the Ru center stays in its Ru(III) state (see Figure 7). It cannot be stated without any doubt if the exchanged ligands are arising from the buffer solution or are due to the binding of apoTf. In view of the more positive shift in energy in the presence of apoTf at the same incubation conditions the ligand exchange is possibly due to an interaction with apoTf. A consecutive binding of carbonate and apoTf to the Ru(III) center is a possible pathway, resulting in a complete dissociation of the four Cl ligands. Because of the changes in the XANES edge shape, both postulated binding modes are feasible and should be taken into consideration. In 2009 an electron paramagnetic resonance (EPR) study on the interaction of **1** with human serum apoTf showed a slow binding of **1** via ligand exchange reactions to the protein.[28] In plasma samples of patients the fraction of **1**/apoTf adducts was smaller than 1%, but in vitro in the absence of other serum proteins the **1**/apoTf adduct formation took place within minutes.[26] The strong binding of **1** to the histidine residues of apoTf was reported from circular dichroism (CD) spectroscopy, electrospray mass spectrometry (ESI-MS), and gel filtration studies.[78] In a X-ray diffraction study the interaction with lactoferrin, a protein closely related to apoTf, could be shown.[79]

Tissue Samples. The XANES spectra collected on tissue samples from mice treated with **1** and **2** are the same (see Figure 5C). **2** is more soluble in water because of its sodium (Na) countercation, and although the pharmacologically active complex anion is identical and biological targets are therefore likely to be the same, it is somewhat less cytotoxic than **1** and differences in their intracellular distribution have been recognized in the past years.[6,26] The spectral features of the XANES spectra from all tissue samples are clearly different from that of solid **1**. Their edge shifts fall into the same energy region as seen for **1** in CS buffer (pH 3.5) up to 4 h of incubation at 37 °C. The XANES spectra bear resemblance to the reference spectra of Ru complexes with $Ru(III)Cl_2ON_3$ or $Ru(III)Cl_2N_4$ active sites. A S ligation in the tissue samples can be ruled out, since all S containing and Ru(II) model compounds are at lower energies. Possible oxidation/coordination assignments are depicted in Figure 7. The two possible first shells $Ru(III)Cl_3N_2(O/N)$, based on model compound data, and $Ru(II)ClN_2(O/N)_3$, derived from theoretical considerations, are the best matching structural motifs. The stepwise release of the Cl ligands throughout the course of application from the original $Ru(III)Cl_4N_2$ over a $Ru(III)Cl_3N_2(O/N)$ to a $Ru(II)ClN_2(O/N)_3$ first shell environment is reasonable. A Ru(II) state would be in agreement with the physiological accessibility of the Ru(III)/Ru(II) redox pair[1] in the presence of a reducing agent and with the activation by reduction mechanism suggested for Ru[30] and other transition metals in cancer therapy like Pt(IV)/Pt(II).[33,80] The favored major average coordination of Ru in tissue is $Ru(III)Cl_3N_2(O/N)$, which is also in agreement with the possible interaction with apoTf in the Ru(III) oxidation state. The micro-XRF distribution maps of Ru in tumor revealed the very good penetration of the drug into all regions of the tissue. Notably, a recent micro-XRF study on **1** and **13** in single SH-SY5Y cells showed a colocalization of the Ru and Fe concentrations inside the cells treated with **1** but not for **13** treated cells.[81] Furthermore, a change in iron distribution after treatment with **1** was seen, which provides further evidence for the interaction of **1** with the Fe homeostasis.

CONCLUSIONS

XAS spectroscopy and micro-XRF were applied to study **1** in vitro and **1**/**2** in vivo. A XAS database of Ru model compounds representing possible coordinations and oxidation states of the Ru metal center was established. The results obtained by fitting theoretical EXAFS amplitudes and phases to the model compounds were in good agreement with the known crystallographic data. The concept of the coordination charge was adopted to correlate the coordination/oxidation environment with the measured energy shifts. This linear correlation was the basis for the assignment of coordination/oxidation states in solution and tissue spectra. XANES analysis on **1** in CS buffer (pH 3.5, 37 °C) suggests the replacement of an average of one Cl ligand through an O atom arising from the buffer solution or a N atom from the deprotonated indazolium countercation. The complex stayed predominantly in this coordination mode up to 4 h. After 8 h of incubation in CS buffer (pH 3.5) a change in the XANES spectra and a strong shift in the edge position by −2.5 eV were observed, pointing toward subsequent changes in the coordination/oxidation state of the Ru center. There is evidence for the release of one or more Cl ligands in carbonate buffer (pH 7.4) to a first coordination shell rich in O and/or N ligands. Under the same

dx.doi.org/10.1021/jm301648f | J. Med. Chem. 2013, 56, 1182−1196

incubation conditions, in the presence of apoTf, a further dissociation of Cl ligands is indicated, and this is a hint for a possible interaction with apoTf. In the presence of GSH two coordination motifs would match the observed edge position: $Ru(II)Cl_3N_2S$ and $Ru(III)ClN_2S_3$. XANES spectra measured on liver and tumor samples, taken from mice treated with **1** and **2**, revealed identical first coordination environments in vivo. The two most probable coordinations are $Ru(III)Cl_3N_2(O/N)$ and $Ru(II)ClN_2(O/N)_3$. The results were independent of the dosages and schedules tested. PCA resulted in a first principal component describing 98% of the variance in all tissue samples. Micro-XRF studies confirmed the high penetration depth of **2** into the closer packed tissue regions. This is the first time coordination/oxidation pairs could be assigned to the drug directly in target tissue.

EXPERIMENTAL SECTION

Sample Preparation. The model compounds were diluted in BN (Sigma Aldrich, CAS 10043-11-5, 99.5%), placed into aluminum sample holders, and sealed with Kapton foil. The BN preparations were prepared for a calculated absorption of about 1 absorbance unit according to standard methods.[82]

The solution samples were prepared by suspending **1** (1 mM), **1** and GSH (0.5:2.5 mM) in 5 mM CS buffer (pH 3.5). **1** in the presence of apoTf (0.5:0.5 mM) and **1** (1 mM) as a reference were suspended in carbonate buffer (pH 7.4), as carbonate is necessary in the binding process to Tf. The resulting suspensions were placed into aluminum sample holders and sealed with Kapton foil. **1** in CS buffer samples were incubated at 37 °C for 30 min, 4 h, and 8 h, respectively. **1** in CS buffer in the presence of GSH was incubated for 5 h at 37 °C. **1** in carbonate buffer (pH 7.4) without and with apoTf was incubated for 30 min at 37 °C. After incubation the samples were flash frozen in liquid nitrogen. The XAS spectra were collected on the flash frozen samples at 20 K.

The tissue samples were taken from experiments performed in accordance with the European Community Guidelines for the use of experimental animals in the animal facility at the Cancer Research Institute, Slovak Academy of Sciences, Bratislava, Slovak Republic, and at the Cancer Research Institute at the Medical University of Vienna, Austria. The tissue material was placed into aluminum sample holders, sealed with Kapton foil, flash frozen in liquid nitrogen, and stored at −80 °C. The following tissue samples were measured: C1-tumor/liver (treated with 15 mg/kg **1**), B2-tumor/liver (7.5 mg/kg **1**), 148-1-tumor/liver (40 mg/kg **2**), B1/F1-liver (40 mg/kg **2**). Details for the buffer preparations and animal tests are given in the Supporting Information.

Part of the tumor (SW480, mouse 148-1) samples from mice treated with **2** were fixed in ethanol and embedded in paraffin according to standard procedures. Consecutively cut thin sections of 5 and 10 μm were prepared. The 5 μm thick sections were mounted on glass slides and stained with H & E. The 10 μm thick sections were mounted on 4 μm thick Ultralene foil fixed on aluminum frames and used for the micro-XRF measurements.

Data Collection and Analysis. The XAS experiments were carried out at beamline BM26A at the European Synchrotron Radiation Facility (ESRF) in Grenoble, France.[83] The model compounds were measured in transmission mode, and the tissue samples and the drug solutions were collected in fluorescence mode. All experiments were conducted at cryogenic temperatures at 20 K. The energy dispersive micro-XRF experiments were conducted at the FLUO beamline at the Angströmquelle Karlsruhe synchrotron (ANKA, Germany) with a spot size of 10 μm.

The program packages ATHENA,[84] ARTEMIS,[84] IFEFFIT,[85] FEFF,[62,63] PySpline,[86] DL-EXCURV,[64,87−89] Sixpack,[72,90,91] and PyMCA[92] were applied for the XAS and micro-XRF data analysis. The pre-edge background was removed by a linear approximation. The normalization was accomplished by fitting a quadratic polynomial (models) or a straight line (tissue and solution samples) to the postedge region. The edge position was determined over the first maximum in the first derivative. The EXAFS analysis followed standard procedures described in refs 82, 85, and 93. The ab initio amplitude and phases were provided by the program packages FEFF7[94] and DL-EXCURV, respectively. The crystallographic values were used as an input for an initial structural model. The EXFAS signals were extracted using ATHENA and PySpline. The DL-EXCURV fits were performed on the k^3-weighted EXAFS signals, and the FEFF7 fits were performed on the back-transform of the first peak in the FT. ARTEMIS and IFEFFIT were used to fit the FEFF7 amplitudes and phases. The program Sixpack was used to perform the PCA, LSF, and LCA in the energy range of 22100−22200 eV. The micro-XRF maps were analyzed with the program package PyMCA.[92] The detailed descriptions of the experimental setups and data extraction and analysis procedures are given in the Supporting Information.

Coordination Charge. The edge positions of XANES spectra are a combination of several features like valence, electronegativity of the first shell atoms, their coordination number, and the formal oxidation state of the central atom. Batsanov[95] introduced the concept of the coordination charge η to account for these factors. With increasing electronegativity of the neighboring atoms the edge positions are shifted to higher energies when the number of ligands stays the same.[69] The coordination charge η is defined as depicted in eq 1.[66]

$$\eta = m - \sum_k n_k c_k \tag{1}$$

where m is the formal oxidation state of the central metal, c_k is the degree of covalence of a bond k, and n_k is the number of such bonds.[66]

The degree of covalence c_k is defined as $1 - I_k$, where I_k is the ionicity of that bond. The ionicity is calculated using Pauling's formula (eq 2)

$$I_k = 1 - \exp\left[-\frac{1}{4}(\chi_M - \chi_L)^2\right] \tag{2}$$

and depends on the electronegativity of the central Ru atom χ_M and the electronegativity of the ligand atom χ_L.[65−69] The coordination charge is calculated as in eq 1 applying I_k calculated as in eq 2.[66,69] The change in electronegativity due to changes in hybridization state was not considered in these calculations.[96,97]

ASSOCIATED CONTENT

Supporting Information

Details on sample preparation, data collection, and analysis; animal test schemes in Table S1; FEFF7 and DL-EXCURV fits in Tables S2 and S3; LCA in Table S4; target transformations in Figure S1; LSF onto tissue samples in Figure S2. This material is available free of charge via the Internet at http://pubs.acs.org.

AUTHOR INFORMATION

Corresponding Author

*Phone: 0043-1-4277-52502. Fax: 0043-1-4277-9525. E-mail: annette.rompel@univie.ac.at.

Notes

The authors declare no competing financial interest.

ACKNOWLEDGMENTS

The research was funded by the Austrian Science Fund (FWF) Grant P23711-N19 (to A.R.), the Fellinger Krebsforschungsverein (to P.H.), and the Genome Austria GENAU Programme (PLACEBO to W.B. and B.K.K.). X-ray absorption experiments were performed at the BM26A beamline within the scope of proposals MD-514 and MD-678 at the European Synchrotron Radiation Facility (ESRF), Grenoble, France. We are grateful to Dr. Sergey Nikitenko at ESRF for providing assistance in using

beamline BM26A. The work was also supported by means of the European Commission FP7 program ELISA. We acknowledge the Synchrotron Light Source ANKA for provision of instruments at the FLUO beamline. Beamtime was granted based on Proposal OTH-88. Prof. Ladislav Novotny and Dr. Peter Rauko (Cancer Research Institute, Slovak Academy of Sciences, Bratislava, Slovak Republic) are acknowledged for providing tumors and organs from in vivo experiments.

■ ABBREVIATIONS USED

ANKA, Angströmquelle Karlsruhe; apoTf, apo-transferrin; BN, boron nitride; CD, circular dichroism; CS, citrate saline; CZE-ICP-MS, capillary zone electrophoresis inductively coupled plasma mass spectrometry; DFT, density functional theory; EPR, electron paramagnetic resonance; ESI-MS, electrospray ionization mass spectrometry; ESRF, European Synchrotron Radiation Facility; eV, electronvolt; EXAFS, extended X-ray absorption fine structure; FT, Fourier transform; GSH, glutathione; H & E, hematoxylin and eosin; HPCE, high performance capillary electrophoresis; HPLC−MS, high performance liquid chromatography−mass spectrometry; LCA, linear combination analysis; LSF, least-squares fitting; micro-XRF, micro X-ray fluorescence; PCA, principal component analysis; pta, 1,3,5-triaza-7-phosphatricyclo[3.3.1.1]decane; RAPTA, ruthenium arene 1,3,5-triaza-7-phosphatricyclo[3.3.1.1]decane; SO_2R^-, sulfinate; SOR^-, sulfenate; SR^-, thiolate; Tf, transferrin; XANES, X-ray absorption near edge structure; XAS, X-ray absorption spectroscopy

■ REFERENCES

(1) Jakupec, M. A.; Galanski, M.; Arion, V. B.; Hartinger, C. G.; Keppler, B. K. Antitumour Metal Compounds: More Than Theme and Variations. *Dalton Trans.* **2008**, *2*, 183−194.

(2) Heffeter, P.; Pongratz, M.; Steiner, E.; Chiba, P.; Jakupec, M. A.; Elbling, L.; Marian, B.; Körner, W.; Sevelda, F.; Micksche, M.; Keppler, B. K.; Berger, W. Intrinsic and Acquired Forms of Resistance against the Anticancer Ruthenium Compound KP1019 [Indazolium *trans*-[Tetrachlorobis(1*H*-indazole)ruthenate (III)] (FFC14A). *J. Pharmacol. Exp. Ther.* **2005**, *312*, 281−289.

(3) Jungwirth, U.; Kowol, C. R.; Keppler, B. K.; Hartinger, C. G.; Berger, W.; Heffeter, P. Anticancer Activity of Metal Complexes: Involvement of Redox Processes. *Antioxid. Redox Signaling* **2011**, *15*, 1085−1128.

(4) Alessio, E.; Mestroni, G.; Bergamo, A.; Sava, G. Ruthenium Antimetastatic Agents. *Curr. Top. Med. Chem.* **2004**, *4*, 1525−1535.

(5) Hartinger, C. G.; Hann, S.; Koellensperger, G.; Sulyok, M.; Groessl, M.; Timerbaev, A. R.; Rudnev, A. V.; Stingeder, G.; Keppler, B. K. Interactions of a Novel Ruthenium-Based Anticancer Drug (KP1019 or FFC14a) with Serum Proteins—Significance for the Patient. *Int. J. Clin. Pharmacol. Ther.* **2005**, *43*, 583−585.

(6) Heffeter, P.; Böck, K.; Atil, B.; Reza Hoda, M.; Körner, W.; Bartel, C.; Jungwirth, U.; Keppler, B.; Micksche, M.; Berger, W.; Koellensperger, G. Intracellular Protein Binding Patterns of the Anticancer Ruthenium Drugs KP1019 and KP1339. *J. Biol. Inorg. Chem.* **2010**, *15*, 737−748.

(7) Mestroni, G.; Alessio, E.; Sava, G. New Salt of Anionic Complexes of Ru(III) as Antimetastatic and Antineoplastic Agents. International Patent PCT C 07F 15/00, A61K 31/28. WO 98/00431, 1998.

(8) Bergamo, A.; Gagliardi, R.; Scarcia, V.; Furlani, A.; Alessio, E.; Mestroni, G.; Sava, G. In Vitro Cell Cycle Arrest, in Vivo Action on Solid Metastasizing Tumors, and Host Toxicity of the Antimetastatic Drug NAMI-A and Cisplatin. *J. Pharmacol. Exp. Ther.* **1999**, *289*, 559−564.

(9) Lipponer, K.-G. Synthese, Charakterisierung, Hydrolyse, Kinetik, Stabilität und Biologische Wirkung Tumorhemmender Ruthenium- und Cobalt-Komplexe. Ph.D. Thesis, Universität Heidelberg, Germany, 1992.

(10) Lipponer, K.-G.; Vogel, E.; Keppler, B. K. Synthesis, Characterization and Solution Chemistry of *trans*-Indazoliumtetrachlorobis(Indazole)Ruthenate(III), a New Anticancer Ruthenium Complex. IR, UV, NMR, HPLC Investigations and Antitumor Activity. Crystal Structures of *trans*-1-Methyl-indazoliumtetrachlorobis-(1-methylindazole)ruthenate(III) and its Hydrolysis Product *trans*-Monoaquatrichlorobis-(1-methylindazole)-ruthenate-(III). *Met.-Based Drugs* **1996**, *3*, 243−260.

(11) Peti, W.; Pieper, T.; Sommer, M.; Keppler, B. K.; Giester, G. Synthesis of Tumor-Inhibiting Complex Salts Containing the Anion *trans*-Tetrachlorobis(indazole)ruthenate(III) and Crystal Structure of the Tetraphenylphosphonium Salt. *Eur. J. Inorg. Chem.* **1999**, *9*, 1551−1555.

(12) Ang, W. H. Development of Organometallic Ruthenium(II) Anticancer (RAPTA) Drugs. *Chimia* **2007**, *61*, 140−142.

(13) Ang, W. H.; Dyson, P. J. Classical and Non-Classical Ruthenium-Based Anticancer Drugs: Towards Targeted Chemotherapy. *Eur. J. Inorg. Chem.* **2006**, *20*, 4003−4018.

(14) Dougan, S. J.; Sadler, P. J. The Design of Organometallic Ruthenium Arene Anticancer Agents. *Chimia* **2007**, *61*, 704−715.

(15) Dyson, P. J. Systematic Design of a Targeted Organometallic Antitumour Drug in Pre-Clinical Development. *Chimia* **2007**, *61*, 698−703.

(16) Peacock, A. F. A.; Sadler, P. J. Medicinal Organometallic Chemistry: Designing Metal Arene Complexes as Anticancer Agents. *Chem. Asian J.* **2008**, *3*, 1890−1899.

(17) Yan, Y. K.; Melchart, M.; Habtemariam, A.; Sadler, P. J. Organometallic Chemistry, Biology and Medicine: Ruthenium Arene Anticancer Complexes. *Chem. Commun.* **2005**, 4764−4776.

(18) Allardyce, C. S.; Dyson, P. J.; Ellis, D. J.; Heath, S. L. [Ru(η6-p-cymene)Cl2(pta)] (pta = 1,3,5-Triaza-7-phosphatricyclo-[3.3.1.1]-decane): A Water Soluble Compound That Exhibits pH Dependent DNA Binding Providing Selectivity for Diseased Cells. *Chem. Commun.* **2001**, *15*, 1396−1397.

(19) Rademaker-Lakhai, J. M.; Van den Bongard, D.; Pluim, D.; Beijnen, J. H.; Schellens, J. H. M. A Phase I and Pharmacological Study with Imidazolium-*trans*-DMSO-imidazole-tetrachlororuthenate, a Novel Ruthenium Anticancer Agent. *Clin. Cancer Res.* **2004**, *10*, 3717−3727.

(20) Hartinger, C. G.; Zorbas-Seifried, S.; Jakupec, M. A.; Kynast, B.; Zorbas, H.; Keppler, B. K. From bench to bedside—Preclinical and Early Clinical Development of the Anticancer Agent Indazolium *trans*-[Tetrachlorobis(1*H*-indazole)ruthenate(III)] (KP1019 or FFC14A). *J. Inorg. Biochem.* **2006**, *100*, 891−904.

(21) Clarke, M. J. Ruthenium Metallopharmaceuticals. *Coord. Chem. Rev.* **2003**, *236*, 209−233.

(22) Sava, G.; Zorzet, S.; Turrin, C.; Vita, F.; Soranzo, M.; Zabucchi, G.; Cocchietto, M.; Bergamo, A.; DiGiovine, S.; Pezzoni, G.; Sartor, L.; Garbisa, S. Dual Action of NAMI-A in Inhibition of Solid Tumor Metastasis. *Clin. Cancer Res.* **2003**, *9*, 1898−1905.

(23) Aitken, J. B.; Levina, A.; A. Lay, P. Studies on the Biotransformations and Biodistributions of Metal-Containing Drugs Using X-Ray Absorption Spectroscopy. *Curr. Top. Med. Chem.* **2011**, *11*, 553−571.

(24) Levina, A.; Mitra, A.; Lay, P. A. Recent Developments in Ruthenium Anticancer Drugs. *Metallomics* **2009**, *1*, 458−470.

(25) Bergamo, A.; Sava, G. Ruthenium Complexes Can Target Determinants of Tumour Malignancy. *Dalton Trans.* **2007**, 1267−1272.

(26) Hartinger, C. G.; Jakupec, M. A.; Zorbas-Seifried, S.; Groessl, M.; Egger, A.; Berger, W.; Zorbas, H.; Dyson, P. J.; Keppler, B. K. KP1019, a New Redox-Active Anticancer Agent—Preclinical Development and Results of a Clinical Phase I Study in Tumor Patients. *Chem. Biodiversity* **2008**, *5*, 2140−2155.

(27) Jakupec, M. A.; Reisner, E.; Eichinger, A.; Pongratz, M.; Arion, V. B.; Galanski, M.; Hartinger, C. G.; Keppler, B. K. Redox-Active Antineoplastic Ruthenium Complexes with Indazole: Correlation of in Vitro Potency and Reduction Potential. *J. Med. Chem.* **2005**, *48*, 2831−2837.
(28) Cetinbas, N.; Webb, M. I.; Dubland, J. A.; Walsby, C. J. Serum−Protein Interactions with Anticancer Ru(III) Complexes KP1019 and KP418 Characterized by EPR. *J. Biol. Inorg. Chem.* **2009**, *15*, 131−145.
(29) Sava, G.; Pacor, S.; Bergamo, A.; Cocchietto, M.; Mestroni, G.; Alessio, E. Effects of Ruthenium Complexes on Experimental Tumors: Irrelevance of Cytotoxicity for Metastasis Inhibition. *Chem.-Biol. Interact.* **1995**, *95*, 109−126.
(30) Schluga, P.; Hartinger, C. G.; Egger, A.; Reisner, E.; Galanski, M.; Jakupec, M. A.; Keppler, B. K. Redox Behavior of Tumor-Inhibiting Ruthenium(iii) Complexes and Effects of Physiological Reductants on Their Binding to GMP. *Dalton Trans.* **2006**, *14*, 1796−1802.
(31) Brindell, M.; Piotrowska, D.; Shoukry, A.; Stochel, G.; Van Eldik, R. Kinetics and Mechanism of the Reduction of (ImH)[*trans*-RuCl4(dmso)(Im)] by Ascorbic Acid in Acidic Aqueous Solution. *J. Biol. Inorg. Chem.* **2007**, *12*, 809−818.
(32) Yano, J.; Yachandra, V. K. X-ray Absorption Spectroscopy. *Photosynth. Res.* **2009**, *102*, 241−254.
(33) Nemirovski, A.; Vinograd, I.; Takrouri, K.; Mijovilovich, A.; Rompel, A.; Gibson, D. New Reduction Pathways for ctc-$[PtCl_2(CH_3CO_2)_2(NH_3)(Am)]$ Anticancer Prodrugs. *Chem. Commun.* **2010**, *46*, 1842−1844.
(34) Best, S. P.; Cheah, M. H. Applications of X-ray Absorption Spectroscopy to Biologically Relevant Metal-Based Chemistry. *Radiat. Phys. Chem.* **2010**, *79*, 185−194.
(35) Penner-Hahn, J. E. X-ray Absorption Spectroscopy in Coordination Chemistry. *Coord. Chem. Rev.* **1999**, *190*, 1101−1123.
(36) Hall, M. D.; Dillon, C. T.; Zhang, M.; Beale, P.; Cai, Z.; Lai, B.; Stampfl, A. P. .; Hambley, T. W. The Cellular Distribution and Oxidation State of Platinum(II) and Platinum(IV) Antitumour Complexes in Cancer Cells. *J. Biol. Inorg. Chem.* **2003**, *8*, 726−732.
(37) Hall, M. D.; Foran, G. J.; Zhang, M.; Beale, P. J.; Hambley, T. W. XANES Determination of the Platinum Oxidation State Distribution in Cancer Cells Treated with Platinum(IV) Anticancer Agents. *J. Am. Chem. Soc.* **2003**, *125*, 7524−7525.
(38) Klein, A. V.; Hambley, T. W. Platinum Drug Distribution in Cancer Cells and Tumors. *Chem. Rev.* **2009**, *109*, 4911−4920.
(39) Hummer, A. A.; Bartel, C.; Arion, V. B.; Jakupec, M. A.; Meyer-Klaucke, W.; Geraki, T.; Quinn, P. D.; Mijovilovich, A.; Keppler, B. K.; Rompel, A. X-ray Absorption Spectroscopy of an Investigational Anticancer Gallium(III) Drug: Interaction with Serum Proteins, Elemental Distribution Pattern, and Coordination of the Compound in Tissue. *J. Med. Chem.* **2012**, *55*, 5601−5613.
(40) Ascone, I.; Meyer-Klaucke, W.; Murphy, L. Experimental Aspects of Biological X-ray Absorption Spectroscopy. *J. Synchrotron Radiat.* **2002**, *10*, 16−22.
(41) Ascone, I.; Strange, R. Biological X-ray Absorption Spectroscopy and Metalloproteomics. *J. Synchrotron Radiat.* **2009**, *16*, 413−421.
(42) Yano, J.; Kern, J.; Irrgang, K.-D.; Latimer, M. J.; Bergmann, U.; Glatzel, P.; Pushkar, Y.; Biesiadka, J.; Lolll, B.; Sauer, K.; Messinger, J.; Zouni, A.; Yachandra, V. K. X-ray Damage to the Mn4Ca Complex in Single Crystals of Photosystem II: A Case Study for Metalloprotein Crystallography. *Proc. Natl. Acad. Sci. U.S.A.* **2005**, *102*, 12047−12052.
(43) Ascone, I.; Messori, L.; Casini, A.; Gabbiani, C.; Balerna, A.; Dell'Unto, F.; Castellano, A. C. Exploiting Soft and Hard X-Ray Absorption Spectroscopy To Characterize Metallodrug/Protein Interactions: The Binding of [*trans*-$RuCl_4$(Im)(dimethylsulfoxide)]-[ImH] (Im = Imidazole) to Bovine Serum Albumin. *Inorg. Chem.* **2008**, *47*, 8629−8634.
(44) Liu, M.; Lim, Z. J.; Gwee, Y. Y.; Levina, A.; Lay, P. A. Characterization of a Ruthenium(III)/NAMI-A Adduct with Bovine Serum Albumin That Exhibits a High Anti-Metastatic Activity. *Angew. Chem., Int. Ed.* **2010**, *49*, 1661−1664.
(45) Sriskandakumar, T.; Petzold, H.; Bruijnincx, P. C. A.; Habtemariam, A.; Sadler, P. J.; Kennepohl, P. Influence of Oxygenation on the Reactivity of Ruthenium−Thiolato Bonds in Arene Anticancer Complexes: Insights from XAS and DFT. *J. Am. Chem. Soc.* **2009**, *131*, 13355−13361.
(46) Salassa, L.; Ruiu, T.; Garino, C.; Pizarro, A. M.; Bardelli, F.; Gianolio, D.; Westendorf, A.; Bednarski, P. J.; Lamberti, C.; Gobetto, R.; Sadler, P. J. EXAFS, DFT, Light-Induced Nucleobase Binding, and Cytotoxicity of the Photoactive Complex *cis*-$[Ru(bpy)_2(CO)Cl]^+$. *Organometallics* **2010**, *29*, 6703−6710.
(47) Salassa, L.; Gianolio, D.; Garino, C.; Salassa, G.; Borfecchia, E.; Ruiu, T.; Nervi, C.; Gobetto, R.; Bizzarri, R.; Sadler, P. J.; Lamberti, C. Structure of $[Ru(bpy)n(AP)(6-2n)]^{2+}$ Homogeneous Complexes: DFT Calculation vs. EXAFS. *J. Phys.: Conf. Ser.* **2009**, *190*, 012141.
(48) Salassa, L.; Garino, C.; Salassa, G.; Nervi, C.; Gobetto, R.; Lamberti, C.; Gianolio, D.; Bizzarri, R.; Sadler, P. J. Ligand-Selective Photodissociation from $[Ru(bpy)(4AP)_4]^{2+}$: A Spectroscopic and Computational Study. *Inorg. Chem.* **2009**, *48*, 1469−1481.
(49) Salassa, L.; Borfecchia, E.; Ruiu, T.; Garino, C.; Gianolio, D.; Gobetto, R.; Sadler, P. J.; Cammarata, M.; Wulff, M.; Lamberti, C. Photo-Induced Pyridine Substitution in *cis*-$[Ru(bpy)_2(py)_2]Cl_2$: A Snapshot by Time-Resolved X-ray Solution Scattering. *Inorg. Chem.* **2010**, *49*, 11240−11248.
(50) Harris, T. V.; Szilagyi, R. K.; McFarlane Holman, K. L. Electronic Structural Investigations of Ruthenium Compounds and Anticancer Prodrugs. *J. Biol. Inorg. Chem.* **2009**, *14*, 891−898.
(51) Keppler, B. K.; Rupp, W.; Juhl, U. M.; Endres, H.; Niebl, R.; Balzer, W. Synthesis, Molecular Structure, and Tumor-Inhibiting Properties of Imidazolium *trans*-Bis(imidazole)tetrachlororuthenate-(III) and Its Methyl-Substituted Derivatives. *Inorg. Chem.* **1987**, *26*, 4366−4370.
(52) Getty, K.; Delgado-Jaime, M. U.; Kennepohl, P. Assignment of Pre-Edge Features in the Ru K-Edge X-ray Absorption Spectra of Organometallic Ruthenium Complexes. *Inorg. Chim. Acta* **2008**, *361*, 1059−1065.
(53) Chao, G. K.-J.; Sime, R. L.; Sime, R. J. The Crystal and Molecular Structure of Tris-acetylacetonatoruthenium(III). *Acta Crystallogr., Sect. B: Struct. Crystallogr. Cryst. Chem.* **1973**, *29*, 2845−2849.
(54) Reynolds, P. A.; Cable, J. W.; Sobolev, A. N.; Figgis, B. N. Structure, Covalence and Spin Polarisation in Tris(acetylacetonato)-ruthenium(III) Studied by X-ray and Polarised Neutron Diffraction. *J. Chem. Soc., Dalton Trans.* **1998**, *4*, 559−570.
(55) Engelhardt, L. M.; Reynolds, P. A.; Sobolev, A. N. Reconciling the Crystal Structure of $[Ru(NH_3)_6]Cl_3$ with Its ESR Properties. *Acta Crystallogr., Sect. C: Cryst. Struct. Commun.* **1995**, *51*, 1045−1047.
(56) Cebrian-Losantos, B.; Reisner, E.; Kowol, C. R.; Roller, A. S.; Arion, V. B.; Keppler, B. K. Synthesis and Reactivity of the Aquation Product of the Antitumor Complex *trans*-$[Ru(III)Cl_4(indazole)_2]^-$. *Inorg. Chem.* **2008**, *47*, 6513−6523.
(57) Pieper, T.; Sommer, M.; Galanski, M.; Keppler, B. K.; Giester, G. $[Ru(III)Cl_3Ind_3]$ and $[Ru(III)Cl_2Ind_4]$: Two New Ruthenium Complexes Derived from the Tumor-Inhibiting Ru(III) Compound HInd (OC-6-11)-$[RuCl_4Ind_2]$ (Ind = Indazole). *Z. Anorg. Allg. Chem.* **2001**, *627*, 261−265.
(58) Engelhardt, L. M.; Reynolds, P. A.; Sobolev, A. N. Reconciling the Crystal Structure of $[Ru(NH_3)_6]Cl_3$ with its ESR Properties. *Acta Crystallogr., Sect. C: Cryst. Struct. Commun.* **1995**, *51*, 1045−1047.
(59) Egger, A.; Arion, V. B.; Reisner, E.; Cebrian-Losantos, B.; Shova, S.; Trettenhahn, G.; Keppler, B. K. Reactions of Potent Antitumor Complex *trans*-$[RuIIICl_4(indazole)_2]^-$ with a DNA-Relevant Nucleobase and Thioethers: Insight into Biological Action. *Inorg. Chem.* **2005**, *44*, 122−132.
(60) Chatt, J.; Leigh, G. J.; Storace, A. P. Complexes of Ruthenium Halides with Organic Sulphides (Thioethers). *J. Chem. Soc. A* **1971**, 1380−1389.
(61) Clark-Baldwin, K.; Tierney, D. L.; Govindaswamy, N.; Gruff, E. S.; Kim, C.; Berg, J.; Koch, S. A.; Penner-Hahn, J. E. The Limitations of X-ray Absorption Spectroscopy for Determining the Structure of

Zinc Sites in Proteins. When Is a Tetrathiolate Not a Tetrathiolate? *J. Am. Chem. Soc.* **1998**, *120*, 8401−8409.
(62) Ankudinov, A. L.; Ravel, B.; Rehr, J. J.; Conradson, S. D. Real-Space Multiple-Scattering Calculation and Interpretation of X-ray-Absorption Near-Edge Structure. *Phys. Rev. B* **1998**, *58*, 7565−7576.
(63) Rehr, J. J.; Albers, R. C. Theoretical Approaches to X-ray Absorption Fine Structure. *Rev. Mod. Phys.* **2000**, *72*, 621−654.
(64) Tomic, S.; Searle, B. G.; Wander, A.; Harrison, M. N.; Dent, A. J.; Mosselmans, J. F. W.; Ingelsfield, J. E. *New Tools for the Analysis of EXAFS: The DL EXCURV Package*; CCLRC Technical Report; Council for the Central Laboratory of the Research Councils: U.K., 2005.
(65) Chen, H. X-ray Absorption Study of Effective Coordination Charges of Iron in Crystals and Amorphous Solids. *J. Phys. Chem. Solids* **1980**, *41*, 641−645.
(66) Cramer, S. P.; Eccles, T. K.; Kutzler, F. W.; Hodgson, K. O.; Mortenson, L. E. Molybdenum X-ray Absorption Edge Spectra. The Chemical State of Molybdenum in Nitrogenase. *J. Am. Chem. Soc.* **1976**, *98*, 1287−1288.
(67) Gupta, M. K. Chemical Shift in the X-ray K Absorption Edge of Strontium. *J. Phys. F: Met. Phys.* **1975**, *5*, 359−362.
(68) Khadikar, P. V.; Pandharkar, S. P. X-ray K-Absorption Edge Analysis of Cobalt in Some Cobalt Complexes. *Jpn. J. Appl. Phys.* **1987**, *26*, 1146−1152.
(69) Wong, J.; Lytle, F. W.; Messmer, R. P.; Maylotte, D. H. K-Edge Absorption Spectra of Selected Vanadium Compounds. *Phys. Rev. B* **1984**, *30*, 5596−5610.
(70) Allred, A. L. Electronegativity Values from Thermochemical Data. *J. Inorg. Nucl. Chem.* **1961**, *17*, 215−221.
(71) Fay, M. J.; Proctor, A.; Hoffmann, D. P.; Houalla, M.; Hercules, D. M. Determination of the Mo Surface Environment of Mo/TiO_2 Catalysts by EXAFS, XANES and PCA. *Microchim. Acta* **1992**, *109*, 281−293.
(72) Webb, S. M. SIXPack a Graphical User Interface for XAS Analysis Using IFEFFIT. *Phys. Scr.* **2005**, *T115*, 1011−2014.
(73) Malinowski, E. R. Theory of error for target factor analysis with applications to mass spectrometry and nuclear magnetic resonance spectrometry. *Anal. Chim. Acta* **1978**, *103*, 339−354.
(74) Küng, A.; Pieper, T.; Wissiack, R.; Rosenberg, E.; Keppler, B. K. Hydrolysis of the tumor-inhibiting ruthenium(III) complexes HIm *trans*-$[RuCl_4(im)_2]$ and HInd *trans*-$[RuCl_4(ind)_2]$ investigated by means of HPCE and HPLC-MS. *J. Biol. Inorg. Chem.* **2001**, *6*, 292−299.
(75) Groessl, M.; Hartinger, C. G.; Dyson, P. J.; Keppler, B. K. CZE-ICP-MS as a Tool for Studying the Hydrolysis of Ruthenium Anticancer Drug Candidates and Their Reactivity towards the DNA Model Compound dGMP. *J. Inorg. Biochem.* **2008**, *102*, 1060−1065.
(76) Graf, N.; Lippard, S. J. Redox Activation of Metal-Based Prodrugs as a Strategy for Drug Delivery. *Adv. Drug Delivery Rev.* **2012**, *64*, 993−1004.
(77) Pongratz, M.; Schluga, P.; Jakupec, M. A.; Arion, V. B.; Hartinger, C. G.; Allmaier, G.; Keppler, B. K. Transferrin Binding and Transferrin-Mediated Cellular Uptake of the Ruthenium Coordination Compound KP1019, Studied by Means of AAS, ESI-MS and CD Spectroscopy. *J. Anal. At. Spectrom.* **2004**, *19*, 46−51.
(78) Timerbaev, A. R.; Hartinger, C. G.; Aleksenko, S. S.; Keppler, B. K. Interactions of Antitumor Metallodrugs with Serum Proteins: Advances in Characterization Using Modern Analytical Methodology. *Chem. Rev.* **2006**, *106*, 2224−2248.
(79) Smith, C. A.; Sutherland-Smith, A. J.; Kratz, F.; Baker, E. N.; Keppler, B. H. Binding of Ruthenium(III) Anti-Tumor Drugs to Human Lactoferrin Probed by High Resolution X-ray Crystallographic Structure Analyses. *J. Biol. Inorg. Chem.* **1996**, *1*, 424−431.
(80) Hall, M. D.; Hambley, T. W. Platinum(IV) Antitumour Compounds: Their Bioinorganic Chemistry. *Coord. Chem. Rev.* **2002**, *232*, 49−67.
(81) Aitken, J. B.; Antony, S.; Weekley, C. M.; Lai, B.; Spiccia, L.; Harris, H. H. Distinct Cellular Fates for KP1019 and NAMI-A Determined by X-ray Fluorescence Imaging of Single Cells. *Metallomics* **2012**, *4*, 1051−1056.
(82) Kelly, S. D.; Hesterberg, D.; Ravel, B. Analysis of Soils and Minerals Using X-ray Absorption Spectroscopy. In *Methods of Soil Analysis. Part 5. Mineralogical Methods*; American Society of Agronomy: Madison, WI, 2008; Vol. *5*, pp 387−463.
(83) Nikitenko, S.; Beale, A. M.; van der Eerden, A. M. J.; Jacques, S. D. M.; Leynaud, O.; O'Brien, M. G.; Detollenaere, D.; Kaptein, R.; Weckhuysen, B. M.; Bras, W. Implementation of a Combined SAXS/WAXS/QuEXAFS Set-Up for Time-Resolved In Situ Experiments. *J. Synchrotron Radiat.* **2008**, *15*, 632−640.
(84) Ravel, B.; Newville, M. ATHENA, ARTEMIS, HEPHAESTUS: Data Analysis for X-ray Absorption Spectroscopy Using IFEFFIT. *J. Synchrotron Radiat.* **2005**, *12*, 537−541.
(85) Newville, M. IFEFFIT: Interactive XAFS Analysis and FEFF Fitting. *J. Synchrotron Radiat.* **2001**, *8*, 322−324.
(86) Tenderholt, A.; Hedman, B.; Hodgson, K. O. Pyspline: A Modern, Cross-Platform Program for the Processing of Raw Averaged XAS Edge and EXAFS Data. In *X-ray Absorption Fine Structure—XAFS 13*; American Institute of Physics: Melville, NY, 2007; Vol. *882*, pp 105−107.
(87) Barth, U.; von; Hedin, L. A Local Exchange-Correlation Potential for the Spin Polarized Case. *J. Phys. C: Solid State Phys.* **1972**, *5*, 1629−1642.
(88) Binsted, N.; Strange, R. W.; Hasnain, S. S. Constrained and Restrained Refinement in EXAFS Data Analysis with Curved Wave Theory. *Biochemistry* **1992**, *31*, 12117−12125.
(89) Stern, E. A. Number of Relevant Independent Points in X-ray-Absorption Fine-Structure Spectra. *Phys. Rev. B* **1993**, *48*, 9825−9827.
(90) Malinowski, E. R. *Factor Analysis in Chemistry*, 2nd ed.; Wiley-Interscience: New York, NY, 1991.
(91) Ressler, T.; Wong, J.; Roos, J.; Smith, I. L. Quantitative Speciation of Mn-Bearing Particulates Emitted from Autos Burning (Methylcyclopentadienyl)manganese Tricarbonyl-Added Gasolines Using XANES Spectroscopy. *Environ. Sci. Technol.* **2000**, *34*, 950−958.
(92) Solé, V. A.; Papillon, E.; Cotte, M.; Walter, P.; Susini, J. A Multiplatform Code for the Analysis of Energy-Dispersive X-ray Fluorescence Spectra. *Spectrochim. Acta, Part B* **2007**, *62*, 63−68.
(93) Bunker, G. *Introduction to XAFS: A Practical Guide to X-ray Absorption Fine Structure Spectroscopy*, 1st ed.; Cambridge University Press: Cambridge, U.K., 2010.
(94) Ankudinov, A. L.; Rehr, J. J. Relativistic Calculations of Spin-Dependent X-ray-Absorption Spectra. *Phys. Rev. B* **1997**, *56*, 1712−1716.
(95) Batsanov, S. S. *Electronegativity of Elements and Chemical Bonds*, 1st ed.; Nauka: Novosibrsk, Russia, 1962.
(96) Hinze, J.; Jaffe, H. H.; Electronegativity., I. Orbital Electronegativity of Neutral Atoms. *J. Am. Chem. Soc.* **1962**, *84*, 540−546.
(97) Hinze, J.; Whitehead, M. A.; Jaffe, H. H. Electronegativity. II. Bond and Orbital Electronegativities. *J. Am. Chem. Soc.* **1963**, *85*, 148−154.